Determining the Complete Stability of Calcite Kink Sites: Real vs Ideal

Blake I. Armstrong,[†] Alessandro Silvestri,[†] Marco De La Pierre,[‡] Paolo Raiteri,[†] and Julian D. Gale[*,†]

†*Curtin Institute for Computation/The Institute for Geoscience Research (TIGeR), School of Molecular and Life Sciences, Curtin University, PO Box U1987, Perth, Western Australia 6845, Australia*

‡*Pawsey Supercomputing Research Centre, Kensington, WA 6151, Australia*

E-mail: J.Gale@curtin.edu.au

Abstract

Kink sites play a pivotal role in the growth and dissolution of materials at the solid-liquid interface. Despite this, little is known about the thermodynamic stability of such sites. Calcium carbonate, in the form of calcite, is one of the most abundant biominerals and a natural means of carbon sequestration in the environment. Here we present a complete determination of the standard free energies for all 16 individual kink sites for the significant case of the calcite $(1\,0\,\bar{1}\,4)$–water interface using both alchemical and pathway-based simulation techniques. The results reveal the importance of distinguishing between real and ideal ion-binding free energies at surfaces, especially for calcite-water where the interfacial potential can alter values by more than 100 kJ/mol per site. Individual kink site stabilities are found to show variations in excess of 60 kJ/mol, which can help explain observed differences in growth rates between the two distinct steps of calcite.

Introduction

Crystallization is a fundamentally important process that leads to the creation of solid materials across all areas of chemistry from pharmaceuticals to geochemistry. Once nucleation has occurred to generate a stable particle, then the competing reactions for crystal growth and dissolution determine how the system evolves. For many materials, particularly when growth is slow, the kink sites at surfaces play a key role as they represent the natural location where matter is added to, or lost from the crystal. As a consequence, kinks have taken center stage in many theories of crystal growth.[1–5] Despite their importance, our understanding of the thermodynamics of individual kink sites is often incomplete. What is known is that the overall stability of the kink sites for a given material for growth from the gas phase is constrained to be equal to the bulk free energy, since removal of a stoichiometric amount from consecutive kink sites returns the solid to the same state, in the limit of an infinitely long step, but with fewer atoms in the bulk. For materials that are growing from solvent,

such as an aqueous solution, then the overall stability instead equates to the dissolution free energy, again with the caveat of an infinitely long step. For the special case of a single component system with only one symmetry-unique type of kink, this implies the stability of the kink is readily determined. However, for the majority of materials the thermodynamics of individual kink sites remains unknown, with no imminent prospect to be able to determine such information experimentally.

One solution to the above challenge is to calculate the free energies of kink sites using computational methods. While this can be routinely achieved for gas phase reactions via energy minimization and lattice dynamics, the situation for growth and dissolution from a solvent is more complex due to the presence of the solid-liquid interface, especially when this involves an ionic solid and a polar solvent. One of the first studies of kink site stability,[6] which examined the barite-water (001) interface, handled this by using the average change in potential energy to estimate the enthalpies of ion binding. Given that addition or removal of ions from the many surface sites is a slow process on the timescale of molecular dynamics, the most popular approach to determine surface-binding thermodynamics in such an environment has been to use bias-enhanced sampling techniques (e.g. metadynamics, umbrella sampling, etc) to reconstruct the free energy landscape. Although feasible, an issue with many such studies to date has been that the free energies are determined for simulation conditions (i.e. a finite concentration in a given periodic cell) and without determining the true concentration (i.e. based on the actual volume explored during the finite length of the simulation), which makes the information hard to connect to actual experimental conditions. In contrast, knowledge of the standard free energy (i.e. at 1 M) would directly yield the equilibrium constant, as well as the thermodynamic driving force for growth or dissolution at any other concentration based on the dependence of the chemical potential of the ions in solution on their activity. Recently, we and others[7,8] have examined the stability of kink sites for NaCl and shown that with care it is possible to determine consistent standard free energies for individual kinks via either of two independent approaches,[9] which paves the way for the study of other more

complex systems, including those that contain molecular fragments rather than just point ions.

One of the materials that has attracted particular attention within the field of crystallization is calcium carbonate ($CaCO_3$), which forms the most abundant biomineral at the Earth's surface and plays an important role in the natural sequestration of carbon dioxide. Calcium carbonate crystallization is also relevant to a diverse range of topics from the mineral support structures of coral reefs and paper production,[10] through to the conservation of limestone buildings and scale formation. Aside from the importance of calcium carbonate as a material, the most stable polymorph at ambient conditions, calcite, has been widely used as a system for the study of crystal growth and interfacial processes in the presence of water. This is because the rhombohedral calcite structure gives rise to stable $(1\,0\,\overline{1}\,4)$ surfaces that often dominate the observed morphology of macroscopically large crystals. Such extended terraces of predominantly clean surfaces have allowed the study of the structure of the calcite-water interface via X-ray reflectivity[11,12] and high resolution atomic force microscopy,[13,14] while the latter also provides considerable information about the dissolution and growth at steps.[15]

The $(1\,0\,\overline{1}\,4)$ surface of calcite can exhibit two kinds of step along the $\langle\overline{4}\,4\,1\rangle$ or $\langle\overline{4}\,8\,1\rangle$ directions at islands or etch pits, named acute and obtuse, which reflect the angles (78° and 102°, respectively) that the cleaved structure makes with the terrace at the step. The symmetry of the structure then gives rise to a total of 16 possible kink sites for propagation of an incomplete step, with 8 for each type of step (see Figure 1, as well as an alternative view given in the supporting information). These 8 different kinks per step are distinguished by the terminating species (Ca or CO_3), the angle at the kink between the end of the row and the surface plane (which can again be either acute or obtuse at the two opposite ends), and finally the carbonate orientation alternates along a step between two possibilities that not only changes its' environment, but also that of the adjacent calcium ions. Specifically, there can be either mono- or bi-dentate coordination of calcium by carbonate along the row. To differentiate these sites we use a notation where each kink is represented by 3 letters (e.g.

AO_b) where the first character indicates whether it is at an acute (A) or obtuse (O) step, the second relates to whether the kink makes an acute or obtuse angle between the end of the row and terrace (again A or O), while the third letter is a, b, c or d, depending on which of the four symmetry-inequivalent ions are present at the kink.

Given the significance of calcite, there have been numerous computational investigations to date of the $(1\,0\,\bar{1}\,4)$ mineral-water interface. While early studies used static approaches with a monolayer of water or continuum models, the majority of work has used molecular dynamics based on classical force fields to examine ion adsorption at the terraces or steps,[16–18] water exchange rates,[19] and the influence on the dynamics of ion binding, or defect formation within the mineral surface. For the specific case of kinks, there have been far fewer studies and there is no complete set of stabilities for all 16 kink sites in contact with bulk water. One of the earliest studies was that of de Leeuw *et al.*,[20] which considered both dry surfaces and molecular dynamics with a monolayer of water. Using internal energy differences, the formation of a pair of kink sites was estimated to cost +103.7 kJ/mol. Subsequently, Kristensen *et al.*[21] performed a comprehensive study of the dry surface using energy minimization leading to energies for 8 different kink pairs that vary between +116 and +212 kJ/mol. Duckworth *et al.*[22] examined the energy to translate an ion pair between kink sites along a dry step edge, which provides information that depends on the stability of pairs of kinks, finding a linear correlation with the logarithm of experimental step velocities for a range of metal carbonates. Significant progress was made by Nielsen Lammers *et al.*[23] who used umbrella sampling to map the free energy for the attachment/detachment of a calcium cation at one of the kink sites on the acute step in the presence of bulk water. Here the objective was the kinetics of cation and water exchange for isotopic fractionation, with the finding that the barrier to add a cation at the carbonate kink was ∼18 kJ/mol to transition from a bridging state close to the top of the step edge to the kink, which is consistent with minima identified at the step edge alone.[18] However, the thermodynamic stability of the kink was not explicitly considered since the free energy was truncated before reaching a plateau in solution.

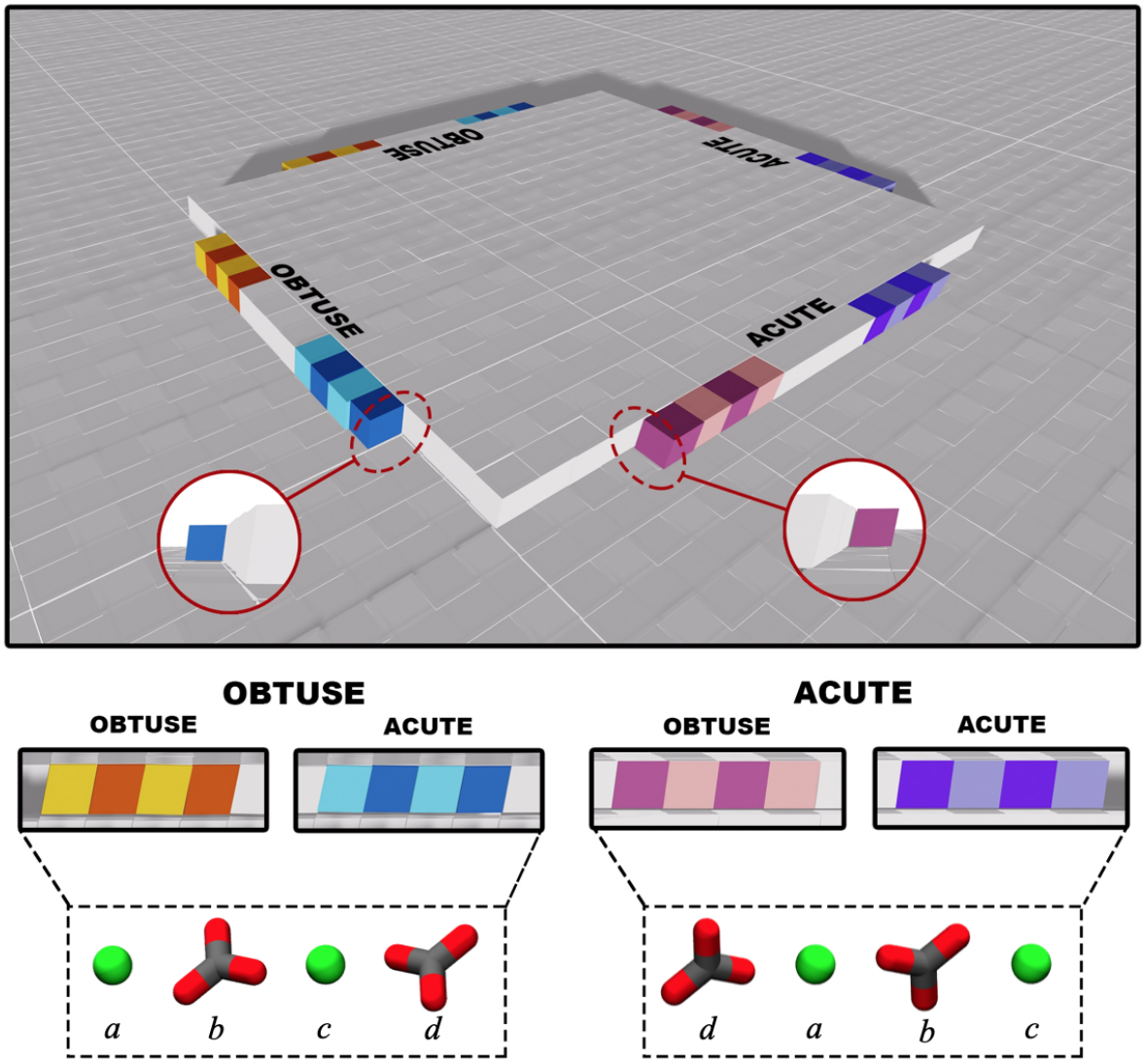

Figure 1: An island on the $(1\,0\,\bar{1}\,4)$ surface of calcite viewed at an angle to the surface showing the 16 possible unique kinks. The four sets of colors (yellow/orange, light/dark blue, light/dark pink, light/dark purple) represent the four types of unique kink (OO, OA, AO, AA), with the dark and light colors representing CO_3^{2-} and Ca^{2+} ions, respectively. Atomistic views of the four ions at the four unique kink types within each set are shown at the bottom of the figure, with arbitrary labels (a, b, c, d) assigned to each ion to simplify referencing each kink ion henceforth. Atoms are colored green, gray and red for calcium, carbon and oxygen, respectively.

Recently, a more comprehensive study of the thermodynamics and mechanisms for kink site formation on calcite has been performed by Broad *et al.*,[24] building on results from a PhD thesis.[25] Here metadynamics was used to examine the free energy surface for 12 of the 16 kinks (all 8 for Ca, but only 4 for CO_3), leading to the proposal of a multistep method for kink site propagation involving multiple ions, rather than simple sequential ion addition. A major advance of this work was that they not only computed the stability of the kinks directly from the metadynamics, but also attempted to correct them to standard conditions by using harmonic walls normal to the surface to restrain the volume of the region explored by ions parallel to the surface. This work found calcium and carbonate ion kink binding free energies in the range of -15 to -31, and -32 to -38 kJ/mol, respectively. Based on their values, the average free energy per ion pair is -58.75 kJ/mol, which should equal the negative bulk dissolution free energy of calcite obtained from the solubility. Unfortunately, this shows a discrepancy of $\sim$10 kJ/mol from experiment (-48.5 kJ/mol) and that expected from the force field used,[26] which was fitted to reproduce experiment. Based on our experience of trying a similar approach previously and finding the same problem, the discrepancy relates to the walls used to restrain the space that the ions can explore parallel to the surface plane being a square of side 6 Å (NB the units were not specified, but are presumed to be consistent with the standard volume quoted). The error arises because the correction to standard conditions assumes that the restrained region is fully explored and well-converged. However, in the presence of water, where diffusion is slower than in the gas phase, this volume is not uniformly sampled, so the correction applied is underestimated. To overcome this, Doudou *et al.*[27] have proposed using a purely harmonic restraint (*i.e.* with zero spacing between the harmonic walls) to reduce the sampling orthogonal to the collective variable, which was shown to resolve this issue for the kink sites of NaCl.[9]

In this study, the objective is the first complete and accurate determination of the stability of all 16 calcite kinks with respect to kink site propagation (i.e. growth or dissolution of an incomplete step), while the study of kink site nucleation (i.e. formation of kinks from

a complete step) is left for future work. It is important to stress upfront that the aim is restricted to obtaining the standard free energies, as validated against the solubility of calcite, rather than examining the mechanistics, which have already been considered for the majority of kink sites in the work of Broad *et al.*.[24]

Methods

To compute the stabilities of ions at the kink sites of calcite we adopt two different approaches, namely the use of alchemical methods (free energy perturbation) to transform an ion at a kink into one in a 1 M ideal solution (a schematic representation of all of the processes involved is given in Figure 2), and pathway-based methods (metadynamics) that explicitly remove an ion from the surface to a point in solution sufficiently far from the kink site. The approaches taken closely follow those previously shown to be successful for the determination of standard free energies for the kink sites of halite (NaCl).[9] However, an important extension for the present study is the need to handle molecular fragments (*e.g.* the carbonate anion). The presence of rotational degrees of freedom for the species at the kink site potentially necessitates changes to the method both for alchemical transformation and removal via a physical pathway. In the case of removing a molecular fragment from a binding site via bias-enhanced sampling, such as metadynamics, it is important to consider whether the species is able to fully sample the rotational orientation configuration space along the pathway. This issue has received extensive consideration in the protein-binding community and so methods involving removal of rotation with orientational restraints, followed by correction for the restricted space sampled, have been proposed.[28] In the case of carbonate, which is a relatively compact molecular entity, no need for such restraints was found to be necessary to obtain satisfactory convergence. However, we note that for other larger molecules this may not be the case and would require validation.

When using alchemical techniques (e.g. free energy perturbation) to remove ions from kinks

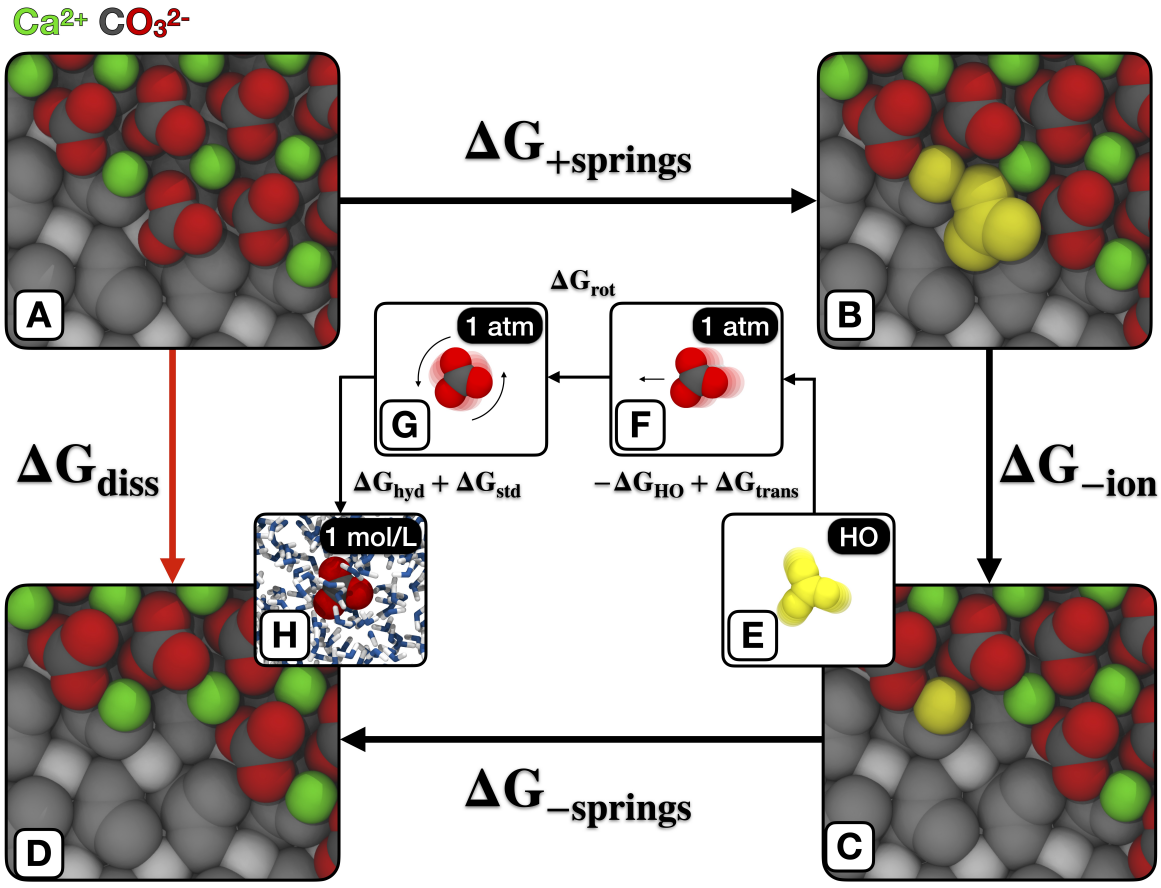

Figure 2: Thermodynamic cycle used to compute the standard free energy of a carbonate kink site with respect to dissolution (ΔG_{diss}) at the calcite $(1\,0\,\bar{1}\,4)$-water interface via an alchemical approach. The same cycle can be used for calcium by neglecting the correction for the free energy of rotation (ΔG_{rot}). Atoms in the island containing the step and kink are colored green, gray and red for calcium, carbon and oxygen, respectively, while the lower terrace atoms are in gray. Atoms that are restrained to their site by a spring to create a harmonic oscillator (HO) are colored yellow. Full details of each step of the thermodynamic cycle can be found in the text.

and transform them into a gas phase species at standard conditions it is also necessary to explicitly consider the molecular nature of the carbonate ion. Here there are essentially two options to choose from when restraining the position of the molecular anion during this transformation: an all-atom (AA) restraint, whereby every atom in the species is restrained at its equilibrium position; or a center-of-mass (COM) restraint, whereby only the center of mass (i.e. carbon atom) of carbonate is restrained to its equilibrium position. In the AA case, the carbonate ion is no longer able to rotate freely, so an analytic correction is needed to account for the change in rotational free energy from a completely restrained ion in vacuum to a freely rotating ion. In the COM case, the carbonate ion is able to rotate freely, so in principle no correction is required. However, it is possible, given the time scale for each FEP window (5 ns), that the full rotational space may not be explored completely as the ion initially has no net rotational motion at the kink and may not fully equilibrate the rotational motion as the interactions are turned off, which could lead to errors in the calculated free energy change. In this work we have chosen to take the AA approach and correct for the rotational free energy, which can be readily calculated using GULP.[29] It should be noted that the considerations here closely parallel those that arise during the Einstein (molecular) crystal approach to determining the free energies of solids.[30,31]

To complete the description of the standard free energy for dissolution of an ion from a kink site, the following steps are included in the thermodynamic cycle shown in Figure 2, where the capital letters in bold refer to the states given in the panels of this figure:

- Addition of harmonic restraints to the ion at the kink site (**A** to **B**), as well as to those ions adjacent to the kink or elsewhere in the system that are found to dissolve during the simulation, as necessary.

- Alchemical removal of the kink site ion by turning off the interactions between the ion and the rest of the system (**B** to **C**).

- Removal of harmonic restraints from all ions except that at the kink site (**C** to **D**), if

any such restraints are present.

- Conversion of an isolated calcium or carbonate ion restrained by all-atom springs to an ideal gas with translational free energy at 1 atm pressure (**E** to **F**): This involves computing the change in the vibrational free energy of the ion, with the intramolecular interactions present for carbonate, when the harmonic restraints are removed ($-\Delta G_{HO}$). Here this term is computed in GULP via energy minimization followed by a vibrational frequency calculation, with Eckart purification to remove the rotational modes in the case where there are no restraints. Because the objective is to reproduce the result of classical molecular dynamics, this free energy is computed without zero point energy or vibrational quantization. Having removed the effect of the restraints, the translational free energy for the ion is added at 1 atm (ΔG_{trans}) based on the ideal gas.

- For carbonate only, addition of the classical rotational free energy uses a symmetry number of 1 (ΔG_{rot}, **F** to **G**).

- Transformation of the ion in the gas phase to become an ion in a 1 M solution (**G** to **H**). Here this involves two contributions; converting the standard state from 1 atm to 1 M (ΔG_{std}), and adding the standard hydration free energy of the ion (ΔG_{hyd}) which was previously determined for the force field being used.[32] Note that the hydration free energies were computed for a single ion in a cubic box, corrected for cell size effects.

Force Field

All calculations were performed using the latest version of our solubility-consistent force field for aqueous metal carbonates[32] that is combined with the flexible, simple point charge water model (SPC/Fw).[33] Importantly, this force field has been fitted against the hydration free energies of Ca^{2+} and CO_3^{2-}, as well as the bulk dissolution free energy of calcite. This is necessary to calculate accurate values for kink ion dissolution free energies as they are intrinsically dependent on this quantity. It should be noted that this force field differs from

the earlier model[26] used by Broad *et al.*,[24] though both reproduce the dissolution free energy of calcite and would therefore be expected to give the same kink standard free energies when averaged over all possible ion pairs. The newer force field gives an improved description of the hydration structure of carbonate and reproduces the more exergonic hydration free energies for metal cations given by Marcus,[34,35] rather than those of David *et al.*.[36]

Molecular dynamics

Molecular dynamics simulations in this work were performed using a combination of the OpenMM[37] and LAMMPS[38] codes. All final values in the main text are from the use of OpenMM, while LAMMPS was used to perform simulations with larger cells to verify that the free energies were converged with respect to system size and reproducible regardless of the choice of code/implementation (see supplementary information for more details of methods for LAMMPS and the results of comparisons). The advantage of using OpenMM over the LAMMPS package, which was used in the foundational work by Silvestri *et al.*,[9] is the ability to utilize GPUs efficiently to run faster and longer simulations.

All of the simulations performed with the OpenMM toolkit for molecular simulation[37] used one GPU in mixed precision with a time step of 1 fs. The Coulomb interactions were calculated using the Particle Mesh Ewald algorithm[39] with an error tolerance of 10^{-5}. The equations of motion were propagated using Langevin dynamics with the LFMiddle discretization.[40] A fully flexible Monte Carlo barostat[41,42] was used to equilibrate the bulk structure of calcite at 1 atm, which was then used to build a calcite slab with two parallel $\{1\,0\,\bar{1}\,4\}$ surfaces. The slab was 10 rows thick (including the top layer with the edge and kink), containing ∼1,212 formula units of $CaCO_3$, repeating in the xy plane, and was constructed such that a step edge could be created running parallel to either the x or y direction of the box to ensure a continuous edge when accounting for periodicity. The 16 different kink site configurations were then constructed such that the edge containing the kink sites had four ion pairs of $CaCO_3$ separating the two kinks. The slab was then hydrated with a total of 2,474

water molecules above and below the slab, followed by equilibration using an anisotropic Monte Carlo barostat[41,42] at 1 atm with only the z axis of the box free to move until the density converged. The lattice parameters were kept fixed at the bulk values in the xy plane to ensure that the center of the slab remained consistent with the bulk structure, while the positions of the ions were free to relax except where otherwise stated. The resulting box was a monoclinic unit cell with lattice parameters of 51.900 Å, 51.900 Å, ∼56 Å, 90.00°, 90.00° and 101.96°.

In preparation for the application of free energy methods, further equilibration was performed in the NVT ensemble for 5 ns to obtain the average positions of Ca^{2+} and CO_3^{2-} within the slab. This is important because harmonic restraints are applied to various ions within the slab during free energy perturbation and metadynamics. If the restrained ions are far from equilibrium, the resulting free energies to add/remove them will be large. Although this is not inherently an issue, the associated larger uncertainties would hinder the precision of the final free energies.

For both free energy methods, a Ca^{2+} in the center of the slab was restrained to prevent drift of the slab throughout the course of a long simulation. Although the center-of-mass motion remover within OpenMM was used, the slab was still observed to drift without this further restraint, which would have otherwise caused errors in the calculated free energies.

Metadynamics

The kink ion dissolution free energies have been calculated using well-tempered metadynamics[43] as implemented in OpenMM through the *Metadynamics* object and analyzed using PLUMED.[44] Six independent walkers[45] were used for a combined simulation time of 300 ns per kink site. Two collective variables (CVs) were used to describe the free energy landscape; the surface normal z-component of the distance between the equilibrium (average) position of the kink ion and the kink ion itself; and the water coordination number of Ca^{2+} being removed from the kink, or the water coordination number of Ca^{2+} underneath the kink ion

being removed in the case of CO_3^{2-}. The water coordination number was described using a switching function (Eq. 1);

$$S(r) = \frac{\text{erfc}(\frac{r-r_0}{a})}{2} \tag{1}$$

where erfc is the complimentary error function, and r_0 and a were 3.1 and 0.45 Å, respectively. Values for this switching function were chosen such that the function at the end of the first hydration shell and the beginning of the second hydration shell of Ca^{2+} has a non-zero first derivative.

Gaussians of widths 0.1 Å and 0.1 were used for the distance and water coordination number CVs, respectively, with an initial height of 2.5 kJ/mol. These were deposited every 1 ps with a bias factor of 8. It was found that this bias factor was sufficient to allow the walkers to freely cross the free energy barriers to explore the CV space completely. All metadynamics simulations were run in the NVT ensemble.

Free energy perturbation

The kink ion dissolution free energies have been computed using a custom implementation of the free energy perturbation technique[46,47] within OpenMM using the Bennett acceptance ratio (BAR) as implemented in pyMBAR.[48] In the description below, bold letters refer to states shown in the schematic figure of the alchemical cycle (Figure 2). The Coulomb interactions between the kink ion and the system were turned off in 30 linearly spaced stages, whilst the van der Waals interactions were turned off in 22 steps according to Equation 2;

$$\lambda_{vdW} = \left(\frac{21-x}{21}\right)^3 \tag{2}$$

where x spans $0-21$ in increments of 1 (**B** to **C**+**E**). Using a polynomial form instead of linear increments placed more λ values around the end of the perturbation, which helped to minimize the standard error of completely decoupling the ion from the system with an

associated large change in free energy. The van der Waals interactions were turned off using a soft core potential (Eq. 3);

$$U(\lambda, r) = 4\epsilon\lambda^n \left[\left(\alpha(1-\lambda)^m + \left(\frac{r}{\sigma}\right)^6 \right)^{-2} - \left(\alpha(1-\lambda)^m + \left(\frac{r}{\sigma}\right)^6 \right)^{-1} \right] \tag{3}$$

using the values of 2, 1 and 0.5 for m, n and α, respectively. Each stage was run for 5 ns at 300 K in the NVT ensemble, with the first 200 ps discarded as equilibration. In total, 51 stages were run (the last Coulomb stage and the first vdW stage overlap), resulting in a combined 255 ns of simulation time per kink ion.

3-Dimensional harmonic restraints were used to restrain the perturbed ions in place to prevent drifting/dissolving, and in the case of perturbing CO_3^{2-} ions, a harmonic restraint was also applied to the adjacent Ca^{2+} ion that is becoming the new kink as the carbonate disappears to prevent it from leaving this site, which was otherwise observed to happen occasionally. These restraints all had a spring constant of 0.75 eVÅ^{-2}, and were added (**A** to **B**) and removed (**C** to **D**) from the system using the same free energy perturbation technique in 11 stages according to Equation 4;

$$\lambda_{HR} = x^5(70x^4 - 315x^3 + 540x^2 - 420x + 126) \tag{4}$$

where x spans $0-1$ in increments of 0.1. Each stage was run for 2.5 ns at 300 K in the NVT ensemble, with the first 200 ps discarded as equilibration for a total simulation time of 27.5 ns. It was found that the free energies obtained with this protocol were well-converged with respect to the results of simulations performed with 48 stages for 5 ns each. The statistical uncertainty on the calculated free energies was obtained from pyMBAR[48] using the asymptotic covariance matrix calculated from singular value decomposition.

Calculation of the interfacial potential

As part of the analysis of the results it was necessary to determine the interfacial potential between calcite and water. To do this, a slab of calcite ∼44 Å thick (1,057 formula units, infinitely repeating in the *xy*-plane) was equilibrated in water in the NP_zT ensemble before running for 10 ns of production in the NVT ensemble. To calculate the change in electrostatic potential between the calcite slab and the aqueous environment, a time-averaged smoothed electrostatic potential grid is calculated by evaluating the reciprocal sum of the smoothed particle-mesh Ewald method over the course of the simulation.[49] The point charges were spread onto a grid with one point per Å in the *xy*-plane, and two points per Å in the *z*-direction. Each atom i contributes to the charge distribution $p_i(r)$ at position r through a spherical Gaussian with a sharpness controlled by an Ewald factor (β) of 0.35 $Å^{-1}$:

$$p_i(r) = q_i \left(\frac{\beta}{\sqrt{\pi}} \right) \mathrm{e}^{-\beta^2 |r - r_i|^2} \tag{5}$$

Results and Discussion

The most widely used approach to determining the stability of ions at mineral-water interfaces is to use bias-enhanced sampling to map the free energy as the ion transfers from the surface to aqueous solution. Hence we first consider the results of this methodology, based on metadynamics, to study the thermodynamics of the kink sites of calcite. It is important to note that there are many potential pitfalls in such calculations including the failure of the collective variable(s) to correctly distinguish between the adsorbed and solution state (e.g. the use of distance alone can lead to the ion binding elsewhere on the surface for large values rather than being in solution), the incorrect mapping of the free energy landscape due to kinetic effects (e.g. slow water exchange at metal cations), and the failure of the free energy curve to reach a plateau in solution due to using a neutral rather than charged slab. A full description of these problems and how to address them for ion-surface binding from liquids

can be found elsewhere.[9]

Central to obtaining the correct standard free energy is the use of a harmonic restraint along a line to ensure that the ion leaves the kink site normal to the surface, which allows the configurational volume explored in solution to be readily determined and the free energy to be referenced to standard conditions. We have previously shown[9] for NaCl that the corrected final free energy difference is independent of the specific choice of spring constant. In addition, it is also necessary to map the free energy as a function of the water coordination number of either the departing ion (in the case of calcium) or the calcium ion below the kink (in the case of carbonate) due to the slow kinetics of water exchange at the kink sites. Examples of both the 2-D and 1-D free energy profiles for a calcium and carbonate kink site are given in Figure 3, while the data for all 16 possible kinks are given in the supplementary information. In line with previous results, the free energy landscape is found to be complex,[23,24] involving multiple minima for the ion to transition from the kink site to solution, or *vice versa*, with the barriers arising from changes in hydration state and distance. Because of the use of a restraint to make the ion leave the surface along a given direction, the route taken is not the actual minimum free energy pathway, and hence any barriers computed here are an upper bound to the true values. Consequently, we focus only on the free energy difference of the initial and final states, rather than the kinetics.

The computed free energies to remove an ion from each possible kink site are given in Table 1 using the notation given in Figure 1 to label the configurations. Considering the free energies for removal of ions along a pathway via metadynamics, there are a wide range of values spanning -23.1 to $+37.1$ kJ/mol for Ca^{2+} and $+9.4$ to $+57.5$ kJ/mol for CO_3^{2-}, which shows that the stability can be particularly sensitive to the local environment, rather than being uniform for all kink sites of the same atom type. This has implications for the growth/dissolution along a row, as certain kinks are more likely to persist for longer. Specifically, for rows dissolving in three of the possible directions (AA, AO and OA) the most probable kink will be a carbonate ion, while for the remaining direction on the obtuse

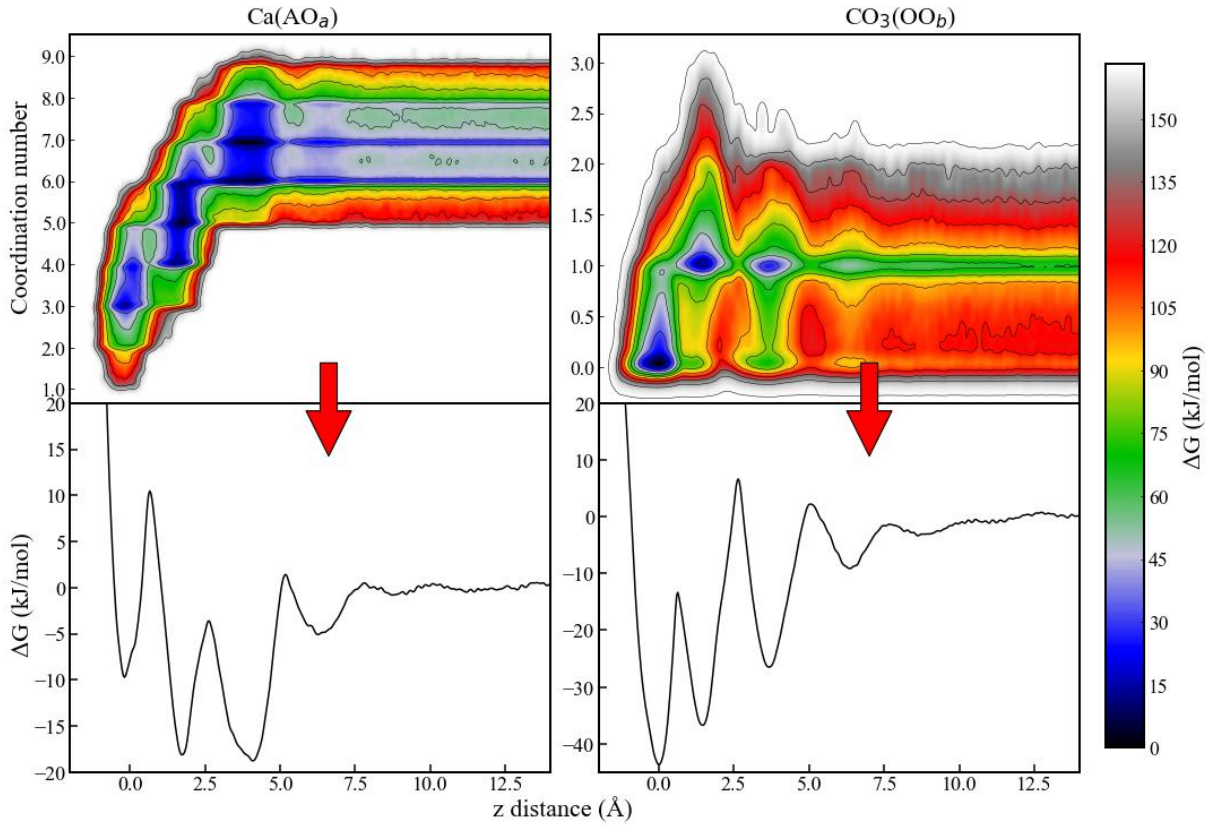

Figure 3: Determination of the standard free energy for ion removal from a kink site via an explicit pathway. The two-dimensional free energy surface is determined as a function of height above the surface (z distance) and the coordination number of calcium by water (for calcium kinks this is for the ion itself, while for carbonate kinks this is for the calcium ion below the kink site). The water coordination number is then integrated out to obtain the 1-D free energy curves from the which the standard free energy change can be determined according to the method of Doudou *et al.*.[27] Representative examples are shown for a calcium (left) and carbonate (right) kink, while the corresponding data for all 16 kink sites can be found in the supporting information.

step (OO) a calcium kink has the greatest stability. In comparison to the work of Broad *et al.*,[24] the range of values here (60.0 and 48.1 kJ/mol for calcium and carbonate, respectively) is much greater (cf. 16 and 6 kJ/mol, again respectively). To support the validity of the numbers computed in this study, we can compare the average values for pairs of kinks per step type and kink direction, and their overall average which should equate to the bulk free energy of dissolution for calcite for the model used (+48.4 kJ/mol). Here the average over all kink pairs is +46.9 ± 2.9 kJ/mol, which represents excellent agreement given that it is hard to reduce the statistical uncertainty below ambient thermal energy. The same quantity determined by summing the kink site free energies obtained by an independent alchemical approach are even closer, being within 0.4 kJ/mol, though noting there is a statistical uncertainty of ± 3.6 kJ/mol. If this data is broken down by step type and direction of the kink (AA, AO, OA, OO) and averaged over the two symmetry-unique types of ion pair per case, then there is a small variation around the overall average dissolution free energy, but when considering the results from both approaches in tandem it is hard to argue that any particular case is distinct with the possible exception of OO, which is consistently the most stable set of kink sites, though the quantitative difference is marginal. A further observation that arises from the close agreement between the average kink site free energies over ion pairs and the bulk dissolution free energy, as well as with the experimental value from solubility measurements (+47.4 kJ/mol),[50] is that suggests that kink site propagation, rather than nucleation, is predominantly responsible for the equilibrium thermodynamics of calcite in an aqueous environment, assuming that nucleation involves less favorable free energies.

Direct comparison of the computed thermodynamics of the individual kink sites to experiment is largely impossible due to the lack of data. However, there have been measurements of the step velocity of calcite as a function of the saturation level,[51] calcium to carbonate activity ratio[51,52] and the presence of a range of background electrolytes.[53] While step velocities are likely to be dominated by step nucleation, rather than propagation, where the latter

Table 1: Standard free energies (kJ/mol) for ion dissolution from calcite kink sites (ΔG^{kink}_{diss}). Values are obtained via both metadynamics (MTD) and free energy perturbation (FEP) at 300 K. Also given is the difference between the MTD and FEP free energies, $\Delta\Delta G^{kink}_{diss}$ (where the averages over ion pairs are given as the mean absolute difference per ion), as well as the free energies for dissolution of ion pairs, both averaged over the 4 possible kinks for each step and direction ($\langle\Delta G_{diss}\rangle$), and over all possible ion pairs ($\langle\langle\Delta G_{diss}\rangle\rangle$), where the latter should be equal to the bulk dissolution free energy. The associated uncertainty (95% confidence) for the individual kink dissolution free energies (ΔG^{kink}_{diss}) obtained via FEP is ± 3.5 and ± 2.5 kJ/mol for $CO_3^{2-}$and Ca^{2+}, respectively; correspondingly, the uncertainty for $\langle\Delta G_{diss}\rangle$ is ± 6.0 kJ/mol, and the uncertainty for $\langle\langle\Delta G_{diss}\rangle\rangle$ is obtained from the deviation of $\langle\Delta G_{diss}\rangle$.

Ion	Kink	ΔG^{kink}_{diss} MTD	FEP	$\Delta\Delta G^{kink}_{diss}$ (MTD – FEP)
Ca^{2+}	AA_a	+5.0	+110.6	−105.7
	AA_c	+10.3	+113.8	−103.5
	AO_a	−23.1	+76.5	−99.7
	AO_c	+21.1	+124.5	−103.4
	OA_a	+24.3	+127.6	−103.3
	OA_c	+14.3	+111.3	−97.0
	OO_a	+32.3	+137.0	−104.7
	OO_c	+37.1	+142.5	−105.4
CO_3^{2-}	AA_b	+33.3	−63.1	+96.4
	AA_d	+39.9	−62.6	+102.5
	AO_b	+39.7	−61.8	+101.5
	AO_d	+57.5	−42.9	+100.5
	OA_b	+33.0	−65.4	+98.4
	OA_d	+22.8	−76.1	+99.0
	OO_b	+17.9	−87.2	+105.1
	OO_d	+9.4	−89.4	+98.7
$\langle\Delta G_{diss}\rangle$	AA	+44.3	+49.3	102.0
	AO	+47.6	+45.9	101.0
	OA	+47.2	+48.7	99.4
	OO	+48.4	+51.4	103.5
$\langle\langle\Delta G_{diss}\rangle\rangle$		+46.9±2.9	+48.8±3.6	101.5±1.7

is more explicitly connected to kink stability, it can be hypothesized that differences in rate may reflect the intrinsic relative stability of ion pairs along the step edges. Acute step growth rates are more sensitive to solution composition,[51] which is consistent with the present finding that the spread of kink site energies is approximately 80 kJ/mol on the acute step, versus only 28 kJ/mol on the obtuse step. Stack and Grantham[52] found that the maximum rate of step propagation was approximately 2.75 times greater for the obtuse step than the acute one. Similarly, Liang *et al.*[54] determined that the obtuse step exhibited faster growth and computed an energy difference between the step types of 22 ± 5 meV (2.1 kJ/mol). Both observations correlate well with the underlying greater stability per ion pair for the obtuse step found here of 2.45 kJ/mol, which if converted into a shift in rate would quantitatively agree with the experimental data. The kink energies also support the observation that a calcium-to-carbonate ratio of greater than 1 should favor growth, as the former ion has a weaker binding free energy on average than carbonate by approximately 16 kJ/mol.

Having considered the kink stability by the widely used approach of removing an ion along a pathway to solution, we can compare the same quantities obtained from alchemical transformation where the ion disappears from the kink and appears in a 1 M solution. From inspection of the free energy perturbation results in Table 1 it is evident that the stability values are radically different from those found by metadynamics. Instead of calcium and carbonate both exhibiting stabilities with an overlapping range, the values are strongly endergonic for calcium, while carbonate is always exergonic. In other words, these values suggest that intrinsically it is hard to remove calcium ions, whereas carbonate would readily dissolve under standard conditions. While at first sight this might indicate that there is something wrong with one of the two methods used here, it can be seen that the range of values for both ions (66 and 46.5 kJ/mol for Ca^{2+} and CO_3^{2-}) is very similar to that found with metadynamics and the trends are also highly correlated; for example, AO_a and OO_d are the most stable sites for calcium and carbonate, respectively, according to both methods, while the least stable sites are also identical.

The reason for the above difference in the two sets of kink stabilities has actually been understood for a long time,[55] though is rarely discussed explicitly in computational studies of ion binding at solid-liquid interfaces for minerals (in contrast to other fields, such as electrocatalysis[56]), namely an interfacial potential shifts the free energy of the ions in the solution phase relative to the solid. When using pathway-based free energy determinations, the ion has to cross the interface, whereas in alchemical methods when the ion transforms from being in the solid to a completely separate solution then this contribution is absent. This difference has been extensively examined by Hünenberger and co-workers in the context of solvation free energies,[57–59] where the interfacial potential from crossing the solvent-vacuum interface changes the value of this quantity. Following this work, the free energy obtained from pathway-based techniques can be labelled as the "real" kink stability, as this relates to the value that would be measured experimentally, should it be possible to determine the thermodynamics for a single ion removal. In contrast, the free energies determined by alchemical methods with respect to a 1 M solution of individual ions (i.e. without ion-ion interactions) can be considered the "ideal" kink stability.

One might ask whether there is any point in knowing the ideal kink stability given that it corresponds to a hypothetical process that cannot be realized experimentally? We argue that it can potentially be of use. For example, if a solid can form an interface with a range of different liquids (e.g. calcite with methanol or water) then knowledge of the ideal kink stabilities for one solvent would allow a first estimate of the values for the other liquid by correcting for the ideal solvation free energies without the need to explicitly simulate the kink sites. In addition, the difference between real and ideal ion binding energies is also relevant to theoretical approaches. While the most popular approach for determining ion binding at solid-liquid interfaces has become bias-enhanced sampling of the pathway for ion to leave or attach to the surface during molecular dynamics, when using quantum mechanical methods it becomes extremely challenging to do this. Therefore it can be necessary to use static approaches to address interfacial binding instead, including for calcite.[60–62] In

other words, a representation of the solid surface is computed with and without the ion, either within periodic boundary conditions to generate a 2D-repeating slab or via a cluster model, to obtain the internal energy difference, which can be extended to the free energy change via adding the phonon contributions. Here solvent effects can be incorporated via continuum solvation approaches, both for finite and periodic systems. Likewise, the (free) energy of the ion after removal can be determined via a continuum solvent model. The key point is to appreciate that the ion binding free energy obtained by such an approach is the same as that obtained by alchemy; namely the ideal binding free energy, rather than the real one. Therefore awareness of the magnitude of the interfacial potential contribution is essential when comparing the results of conventional quantum mechanical approaches based on energy minimization and lattice dynamics versus the outcome of pathway-based molecular dynamics. Given the large difference between the real and ideal stabilities of calcite kinks, and quite probably many other mineral-water sites, it is vital that equivalent definitions of the free energy are being compared.

Having proposed that the difference in the kink site stabilities between metadynamics and free energy perturbation is due to the presence of an interfacial potential it is important to examine whether this is indeed the case. Here we have performed a simulation to directly compute this quantity for the calcite $(1\,0\,\overline{1}\,4)$-water interface. In Table 1, the difference between the real and ideal standard free energies is given for each kink site. While there is some variation in the absolute magnitude per site (*i.e.* < 9 kJ/mol), the scatter is largely within the statistical uncertainty of the method. Importantly, the sign of the free energy difference is inverted between calcium and carbonate, consistent with a potential shift multiplied by the charge of the ion (*i.e.* qV). Quantitatively, the average potential per kink derived from the thermodynamics of ion removal is -0.53 V. In comparison, the directly computed potential for the calcite $(1\,0\,\overline{1}\,4)$-water interface, as shown in Figure 4, is -0.97 ± 0.05 V. While initially this might suggest a large quantitative disagreement, the direct calculation of the interfacial potential was conducted on a flat $(1\,0\,\overline{1}\,4)$ surface: This is because

it is easier to obtain a reliable result here, as the potential is averaged across the surface plane to improve the statistical convergence of the curve normal to the interface. A kink is situated within an island above the terrace and therefore has partially crossed the region over which the potential changes between calcite and bulk water. This is consistent with the actual potential experienced being less than the full value, which represents the upper bound. Indeed, as a kink represents a site that is halfway between the bulk and solution, the fact that the interfacial potential experienced is close to 50% of the full value appears physically reasonable. For comparison, the same effect when computed for kink sites at the NaCl (0 0 1)-water interface is only -0.042 V,[9] versus the interfacial potential for NaCl (001)-water when computed directly being -0.088 ± 0.008 V (see supporting information), which is again consistent with the kinks experiencing approximately half of the value for the flat surface.

While there is little information regarding the interfacial potential for mineral-water systems in the literature, there has been investigation of the water-vacuum boundary.[63] Sokhan and Tildesley[64] determined the corresponding interfacial potentials for this case for a range of water models. Although the force field used here (SPC/Fw) was not available at the time, similar models (SPC and SPC/E) had interfacial potentials of -0.53 and -0.55 V, respectively. This makes this contribution very similar to that at a calcite kink, though approximately half the value at the terraces. For the water-vacuum interface, the origin of the interfacial potential is due to the net average orientation of the water dipoles at the liquid surface. Similarly, the calcite $(1\,0\,\bar{1}\,4)$-water interface is also known to have at least two well-defined ordered water layers with a strong orientational preference that maximizes the interaction of molecules with the exposed ions in the underlying surface.[11,12,14] Hence, there is a strong physical justification for the presence of such a large interfacial potential at the calcite-water interface.

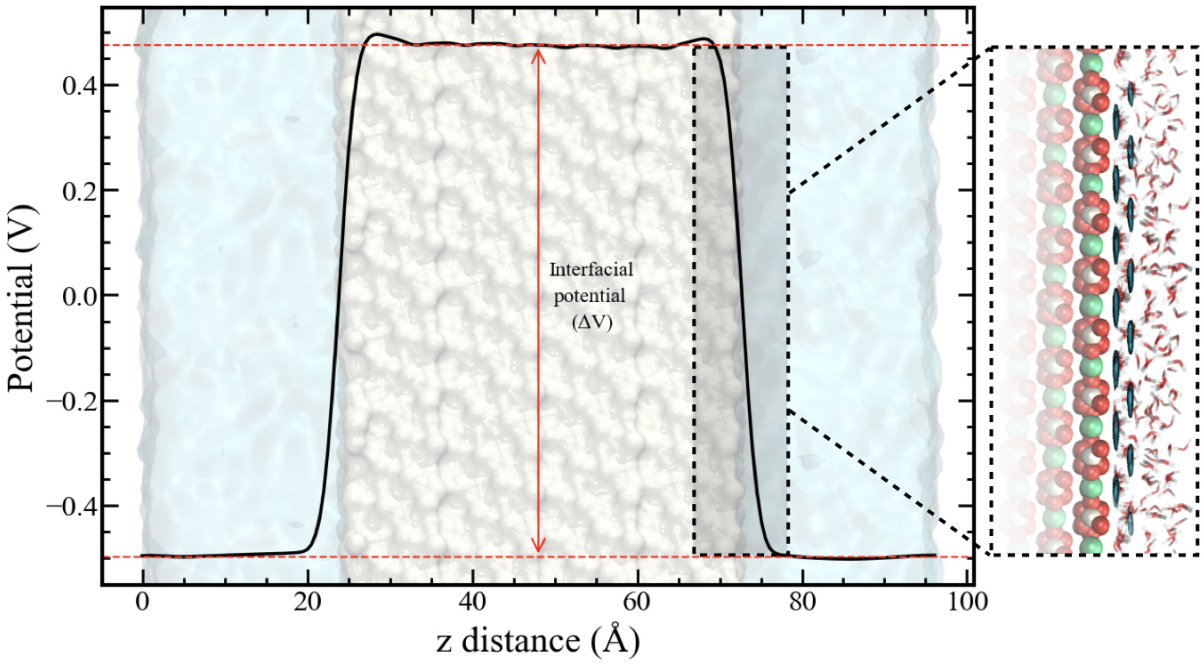

Figure 4: Electrostatic potential as a function of the surface normal z coordinate averaged over the course of 10 ns for a ∼47 Å thick slab of calcite equilibrated in contact with 1,057 water molecules. Three replicates were conducted, resulting in a calculated interfacial potential of 0.97 ± 0.05 V (presented as a 95% confidence interval). The graph has been underlaid with a semi-transparent render of the calcite slab (gray)/water (blue) system to indicate the physical location of the two components within the system. To the right of the graph is an image of the calcite-water interface within the dashed box demonstrating the two ordered water layers on the calcite surface. The dark cyan ellipses represent a time-averaged 3D density map of the water oxygen atoms in the ordered layers. The green, red and white spheres within the calcite slab are the calcium, oxygen and carbon elements, respectively. The red and white in the line representation of water above the surface from a single time frame corresponds to oxygen and hydrogen, respectively.

Conclusion

In this study we have shown that it is now possible to reliably determine the free energies for kink sites of ionic materials, such as minerals, at the interface with water, and in principle any solvent. This includes cases where the ions are no longer simple point charges, but can be molecular entities, such as carbonate. However, the significance is much broader since the same methodology is also applicable to any site at a crystal surface-fluid interface. This means that it will be possible in future to accurately determine the thermodynamics for other binding events that are relevant to crystal growth with confidence, even in the absence of the validation against the bulk dissolution free energy, as is the case for kinks. In particular, both the real and ideal free energies to add ions to step edges or terraces can be computed, which provide insights into the nucleation of a new row or layer, and thereby overall step or crystal propagation, respectively. Knowledge of the thermodynamics of individual surface sites also provides a valuable input for more macroscopic simulations of crystal growth, such as those based on kinetic theories[65] or Monte Carlo techniques that focus on the addition or removal of growth units.[66] For calcite, this removes the need to assume either a single estimated kink energy for all sites in such simulations,[67] or even the grouping into 4 distinct sets.[68] While the current scheme is focused on solely determining the standard real and/or ideal free energy for ion binding at interfaces, the future extension of the method to the calculation of the rate constants through the use of enhanced sampling approaches[69,70] should provide a full picture of crystal growth at the surface of important systems, such as calcite.

Supporting Information Available

The Supporting Information is available free of charge at http:pubs.acs.org.

Calcite surface structure. Methods for LAMMPS simulations. Free energy surfaces for restrained ion removal from kink sites at the calcite $(1\,0\,\bar{1}\,4)$-water interface. Components of the standard free energies for the alchemical cycle computed with OpenMM. Ideal kink site

stabilities computed using LAMMPS. Ion pair stabilities at kink sites. Interfacial potential at the halite (0 0 1)-water interface.

Acknowledgement

The Australian Research Council is acknowledged for funding under grant FL180100087, as well as the Pawsey Supercomputing Centre and National Computational Infrastructure for provision of computational resources.

References

(1) Kossel, W. Zur Theorie des Kristallwachstums. *Nachrichten von der Gesellschaft der Wissenschaften zu Göttingen, Mathematisch-Physikalische Klasse* **1927**, *1927*, 135–143.

(2) Stranski, I. N. Zur Theorie des Kristallwachstums. *Zeitschrift für Physikalische Chemie* **1928**, *136U*, 259–278.

(3) Burton, W. K.; Cabrera, N.; Frank, F. C.; Mott, N. F. The Growth of Crystals and the Equilibrium Structure of their Surfaces. *Philosophical Transactions of the Royal Society of London. Series A, Mathematical and Physical Sciences* **1951**, *243*, 299–358.

(4) Nielsen, A. E.; Toft, J. M. Electrolyte crystal growth kinetics. *Journal of Crystal Growth* **1984**, *67*, 278–288.

(5) Nielsen, A. E. Electrolyte crystal growth mechanisms. *Journal of Crystal Growth* **1984**, *67*, 289–310.

(6) Stack, A. G. Molecular dynamics simulations of solvation and kink site formation at the 001 barite-water surface. *Journal of Physical Chemistry C* **2009**, *113*, 2104–2110.

(7) Joswiak, M. N.; Doherty, M. F.; Peters, B. Ion Dissolution Mechanism and Kinetics at Kink Sites on NaCl Surfaces. *Proceedings of the National Academy of Sciences* **2018**, *115*, 656–661.

(8) Joswiak, M. N.; Peters, B.; Doherty, M. F. In Silico Crystal Growth Rate Prediction for NaCl from Aqueous Solution. *Crystal Growth & Design* **2018**, *18*, 6302–6306.

(9) Silvestri, A.; Raiteri, P.; Gale, J. D. Obtaining Consistent Free Energies for Ion Binding at Surfaces from Solution: Pathways versus Alchemy for Determining Kink Site Stability. *Journal of Chemical Theory and Computation* **2022**, *18*, 5901–5919.

(10) Kang, D. S.; Han, J. S.; Choi, J. S.; Seo, Y. B. Development of Deformable Calcium Carbonate for High Filler Paper. *ACS Omega* **2020**, *5*, 15202–15209.

(11) Fenter, P.; Kerisit, S.; Raiteri, P.; Gale, J. D. Is the Calcite-Water Interface Understood? Direct Comparisons of Molecular Dynamics Simulations with Specular X-ray Reflectivity Data. *Journal of Physical Chemistry C* **2013**, *117*, 5028–5042.

(12) Brugman, S. J. T.; Raiteri, P.; Accordini, P.; Megens, F.; Gale, J. D.; Vlieg, E. Calcite (104) Surface–Electrolyte Structure: A 3D Comparison of Surface X-ray Diffraction and Simulations. *Journal of Physical Chemistry C* **2020**, acs.jpcc.0c04094.

(13) Söngen, H.; Reischl, B.; Miyata, K.; Bechstein, R.; Raiteri, P.; Rohl, A. L.; Gale, J. D.; Fukuma, T.; Kühnle, A. Resolving Point Defects in the Hydration Structure of Calcite (10.4) with Three-Dimensional Atomic Force Microscopy. *Physical Review Letters* **2018**, *120*, 116101.

(14) Söngen, H.; Schlegel, S. J.; Jaques, Y. M.; Tracey, J.; Hosseinpour, S.; Hwang, D.; Bechstein, R.; Bonn, M.; Foster, A. S.; Kühnle, A. et al. Water orientation at the calcite-water interface. *Journal of Physical Chemistry Letters* **2021**, *12*, 7605–7611.

(15) Ruiz-Agudo, E.; Putnis, C. V. Direct observations of mineral fluid reactions using atomic force microscopy: the specific example of calcite. *Mineralogical Magazine* **2018**, *76*, 227–253.

(16) Kerisit, S.; Parker, S. C. Free energy of adsorption of water and metal ions on the $\{1\,0\,\bar{1}\,4\}$ calcite surface. *Journal of the American Chemical Society* **2004**, *126*, 10152–10161.

(17) Aufort, J.; Schuitemaker, A.; Green, R.; Demichelis, R.; Raiteri, P.; Gale, J. D. Determining the Adsorption Free Energies of Small Organic Molecules and Intrinsic Ions at the Terrace and Steps of Calcite. *Crystal Growth and Design* **2022**, *22*, 1455–1458.

(18) De La Pierre, M.; Raiteri, P.; Stack, A. G.; Gale, J. D. Uncovering the Atomistic Mechanism for Calcite Step Growth. *Angewandte Chemie - International Edition* **2017**, *56*, 8464–8467.

(19) De La Pierre, M.; Raiteri, P.; Gale, J. D. Structure and Dynamics of Water at Step Edges on the Calcite $\{1\,0\,\bar{1}\,4\}$ Surface. *Crystal Growth and Design* **2016**, *16*, 5907–5914.

(20) De Leeuw, N. H.; Parker, S. C.; Harding, J. H. Molecular dynamics simulation of crystal dissolution from calcite steps. *Physical Review B* **1999**, *60*, 13792–13799.

(21) Kristensen, R.; Stipp, S. L. S.; Refson, K. Modeling Steps and Kinks on the Surface of Calcite. *Journal of Chemical Physics* **2004**, *121*, 8511–8523.

(22) Duckworth, O. W.; Cygan, R. T.; Martin, S. T. Linear Free Energy Relationships between Dissolution Rates and Molecular Modeling Energies of Rhombohedral Carbonates. *Langmuir* **2004**, *20*, 2938–2946.

(23) Lammers, L. N.; Kulasinski, K.; Zarzycki, P.; DePaolo, D. J. Molecular simulations of kinetic stable calcium isotope fractionation at the calcite-aqueous interface. *Chemical Geology* **2020**, *532*, 119315.

(24) Broad, A.; Darkins, R.; Duffy, D. M.; Ford, I. J. Calcite Kinks Grow via a Multistep Mechanism. *The Journal of Physical Chemistry C* **2022**, *126*, 15980–15985.

(25) Darkins, R. D. W. Computational Insight into the Molecular Mechanisms that Control the Growth of Inorganic Crystals. Ph.D. thesis, University College London, 2016.

(26) Raiteri, P.; Demichelis, R.; Gale, J. D. Thermodynamically Consistent Force Field for Molecular Dynamics Simulations of Alkaline-Earth Carbonates and Their Aqueous Speciation. *The Journal of Physical Chemistry C* **2015**, *119*, 24447–24458.

(27) Doudou, S.; Burton, N. A.; Henchman, R. H. Standard Free Energy of Binding from a One-Dimensional Potential of Mean Force. *Journal of Chemical Theory and Computation* **2009**, *5*, 909–918.

(28) Gilson, M. K.; Given, J. A.; Bush, B. L.; McCammon, J. A. The Statistical-Thermodynamic Basis for Computation of Binding Affinities: A Critical Review. *Biophysical Journal* **1997**, *72*, 1047–1069.

(29) Gale, J. D.; Rohl, A. L. The General Utility Lattice Program (GULP). *Molecular Simulation* **2003**, *29*, 291–341.

(30) Frenkel, D.; Ladd, A. J. C. New Monte Carlo Method to Compute the Free Energy of Arbitrary Solids. Application to the fcc and hcp Phases of Hard Spheres. *The Journal of Chemical Physics* **1984**, *81*, 3188.

(31) Vega, C.; Noya, E. G. Revisiting the Frenkel-Ladd method to compute the free energy of solids: The Einstein molecule approach. *The Journal of Chemical Physics* **2007**, *127*, 154113.

(32) Armstrong, B.; Silvestri, A.; Demichelis, R.; Raiteri, P.; Gale, J. D. Solubility-consistent force field simulations for aqueous metal carbonate systems using GPUs. *Philosophical Transactions of the Royal Society A* **2023**, *381*, 202220250.

(33) Wu, Y.; Tepper, H. L.; Voth, G. A. Flexible simple point-charge water model with improved liquid-state properties. *Journal of Chemical Physics* **2006**, *124*, 024503.

(34) Marcus, Y. A simple empirical model describing the thermodynamics of hydration of ions of widely varying charges, sizes, and shapes. *Biophysical chemistry* **1994**, *51*, 111 – 127.

(35) Marcus, Y. *Ions in Solution and Their Solvation*; John Wiley & Sons, Inc, 2015; pp 113–115.

(36) David, F.; Vokhmin, V.; Ionova, G. Water characteristics depend on the ionic environment. Thermodynamics and modelisation of the aquo ions. *Journal of Molecular Liquids* **2001**, *90*, 45–62.

(37) Eastman, P.; Swails, J.; Chodera, J. D.; McGibbon, R. T.; Zhao, Y.; Beauchamp, K. A.; Wang, L.; Simmonett, A. C.; Harrigan, M. P.; Stern, C. D. et al. OpenMM 7: Rapid Development of High Performance Algorithms for Molecular Dynamics. *PLoS Comput. Biol.* **2017**, *13*, e1005659.

(38) Plimpton, S. Fast Parallel Algorithms for Short-Range Molecular Dynamics. *Journal of Computational Physics* **1995**, *117*, 1–19.

(39) Essmann, U.; Perera, L.; Berkowitz, M. L.; Darden, T.; Lee, H.; Pedersen, L. G. A smooth particle mesh Ewald method. *The Journal of Chemical Physics* **1995**, *103*, 8577–8593.

(40) Zhang, Z.; Liu, X.; Yan, K.; Tuckerman, M. E.; Liu, J. Unified Efficient Thermostat Scheme for the Canonical Ensemble with Holonomic or Isokinetic Constraints via Molecular Dynamics. *Journal of Physical Chemistry A* **2019**, *123*, 6056–6079.

(41) Chow, K. H.; Ferguson, D. M. Isothermal-isobaric molecular dynamics simulations with Monte Carlo volume sampling. *Computer Physics Communications* **1995**, *91*, 283–289.

(42) Åqvist, J.; Wennerström, P.; Nervall, M.; Bjelic, S.; Brandsdal, B. O. Molecular dynamics simulations of water and biomolecules with a Monte Carlo constant pressure algorithm. *Chemical Physics Letters* **2004**, *384*, 288–294.

(43) Barducci, A.; Bussi, G.; Parrinello, M. Well-Tempered Metadynamics: A Smoothly Converging and Tunable Free-Energy Method. *Physical Review Letters* **2008**, *100*, 20603.

(44) Bonomi, M.; Bussi, G.; Camilloni, C.; Tribello, G. A.; Banas, P.; Barducci, A.; Bernetti, M.; Bolhuis, P. G.; Bottaro, S.; Branduardi, D. et al. Promoting Transparency and Reproducibility in Enhanced Molecular Simulations. *Nature Methods* **2019**, *16*, 670–673.

(45) Raiteri, P.; Laio, A.; Gervasio, F. L.; Micheletti, C.; Parrinello, M. Efficient Reconstruction of Complex Free Energy Landscapes by Multiple Walkers Metadynamics. *Journal of Physical Chemistry B* **2006**, *110*, 3533–3539.

(46) Kirkwood, J. G. Statistical mechanics of fluid mixtures. *The Journal of Chemical Physics* **1935**, *3*, 300–313.

(47) Zwanzig, R. W. High-Temperature Equation of State by a Perturbation Method. I. Nonpolar Gases. *Journal of Chemical Physics* **1954**, *22*, 1420–1426.

(48) Shirts, M. R.; Chodera, J. D. Statistically optimal analysis of samples from multiple equilibrium states. *Journal of Chemical Physics* **2008**, *129*, 124105.

(49) Aksimentiev, A.; Schulten, K. Imaging α-Hemolysin with Molecular Dynamics: Ionic Conductance, Osmotic Permeability, and the Electrostatic Potential Map. *Biophysical Journal* **2005**, *88*, 3745–3761.

(50) Plummer, L. N.; Busenberg, E. The solubilities of calcite, aragonite and vaterite in

CO_2-H_2O solutions between 0 and 90^{o}C, and an evaluation of the aqueous model for the system $CaCO_3$-CO_2-H_2O. *Geochimica et Cosmochimica Acta* **1982**, *46*, 1011–1040.

(51) Larsen, K.; Bechgaard, K.; Stipp, S. L. S. The effect of the Ca^{2+} to CO_3^{2-} activity ratio on spiral growth at the calcite 10-14 surface. *Geochimica et Cosmochimica Acta* **2010**, *74*, 2099–2109.

(52) Stack, A. G.; Grantham, M. C. Growth Rate of Calcite Steps As a Function of Aqueous Calcium-to-Carbonate Ratio: Independent Attachment and Detachment of Calcium and Carbonate Ions. *Crystal Growth and Design* **2010**, *10*, 1409–1413.

(53) Ruiz-Agudo, E.; Putnis, C. V.; Wang, L.; Putnis, A. Specific effects of background electrolytes on the kinetics of step propagation during calcite growth. *Geochimica et Cosmochimica Acta* **2011**, *75*, 3803–3814.

(54) Liang, Y.; Baer, D. R.; McCoy, J. M.; Amonette, J. E.; LaFemina, J. P. Dissolution kinetics at the calcite-water interface. *Geochimica et Cosmochimica Acta* **1996**, *60*, 4883–4887.

(55) Hush, N. S. The Free Energies of Hydration of Gaseous Ions. *Australian Journal of Scientific Research* **1948**, *1*, 480–494.

(56) Zeradjanin, A. R.; Spanos, I.; Masa, J.; Rohwerder, M.; Schlögl, R. Perspective on experimental evaluation of adsorption energies at solid/liquid interfaces. *Journal of Solid State Electrochemistry* **2021**, *25*, 33–42.

(57) Kastenholz, M. A.; Hünenberger, P. H. Computation of Methodology-Independent Ionic Solvation Free Energies from Molecular Simulations. I. The Electrostatic Potential in Molecular Liquids. *The Journal of Chemical Physics* **2006**, *124*, 124106.

(58) Kastenholz, M. A.; Hünenberger, P. H. Computation of Methodology-Independent Ionic

Solvation Free Energies from Molecular Simulations. II. The Hydration Free Energy of the Sodium Cation. *The Journal of Chemical Physics* **2006**, *124*, 224501.

(59) Reif, M. M.; Hünenberger, P. H. Computation of Methodology-Independent Ionic Solvation Free Energies from Molecular Simulations. III. Correction terms for the solvation free energies, enthalpies, entropies, heat capacities, volumes, compressibilities, and expansivities of solvated ions. *The Journal of Chemical Physics* **2011**, *134*, 144103.

(60) Ruuska, H.; Hirva, P.; Pakkanen, T. A. Cluster Models for Calcite Surfaces: Ab Initio Quantum Chemical Studies. *The Journal of Physical Chemistry B* **1999**, *103*, 6734–6740.

(61) Andersson, M. P.; Stipp, S. L. S. How acidic is water on calcite? *The Journal of Physical Chemistry C* **2012**, *116*, 18779–18787.

(62) Andersson, M. P.; Rodriguez-Blanco, J. D.; Stipp, S. L. S. Is bicarbonate stable in and on the calcite surface? *Geochimica et Cosmochimica Acta* **2016**, *176*, 198–205.

(63) Leung, K. Surface Potential at the Air–Water Interface Computed Using Density Functional Theory. *Journal of Physical Chemistry Letters* **2010**, *1*, 496–499.

(64) Sokhan, V. P.; Tildesley, D. J. The Free Surface of Water: Molecular Orientation, Surface Potential and Nonlinear Susceptibility. *Molecular Physics* **1997**, *92*, 625–640.

(65) Nielsen, L. C.; DePaolo, D. J.; De Yoreo, J. J. Self-consistent ion-by-ion growth model for kinetic isotopic fractionation during calcite precipation. *Geochimica Cosmochimica Acta* **2012**, *86*, 166–181.

(66) Anderson, M. W.; Gebbie-Rayet, J. T.; Hill, A. R.; Farida, N.; Attfield, M. P.; Cubillas, P.; Blatov, V. A.; Proserpio, D. M.; Akporiaye, D.; Arstad, B. et al. Predicting crystal growth via a unified kinetic three-dimensional partition model. *Nature* **2017**, *544*, 456–459.

(67) De Yoreo, J. J.; Zepeda-Ruiz, L. A.; Friddle, R. W.; Qiu, S. R.; Wasylenki, L. E.; Chernov, A. A.; Gilmer, G. H.; Dove, P. M. Rethinking Classical Crystal Growth Models through Molecular Scale Insights: Consequences of Kink-Limited Kinetics. *Crystal Growth and Design* **2009**, *9*, 5135–5144.

(68) Kurganskaya, I.; Luttge, A. Kinetic Monte Carlo Approach to Study Carbonate Dissolution. *The Journal of Physical Chemistry C* **2016**, *120*, 6482–6492.

(69) Dellago, C.; Bolhuis, P. G.; Csajka, F. S.; Chandler, D. Transition path sampling and the calculation of rate constants. *Journal of Chemical Physics* **1998**, *108*, 1964–1977.

(70) Allen, R. J.; Valeriani, C.; ten Wolde, P. R. Forward flux sampling for rare event simulations. *Journal of Physics: Condensed Matter* **2009**, *21*, 463102.

TOC Graphic

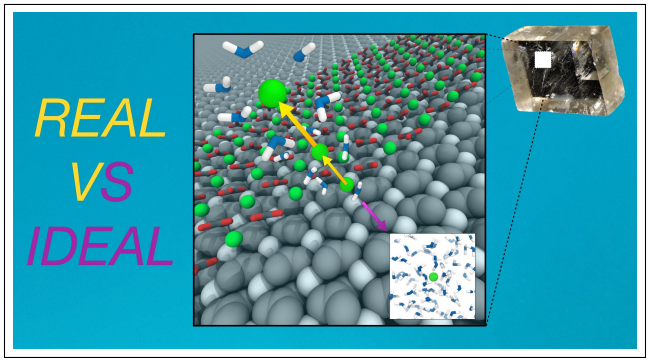

Supporting Information: Determining the Complete Stability of Calcite Kink Sites: Real vs Ideal

Blake I. Armstrong,[†] Alessandro Silvestri,[†] Marco De La Pierre,[‡] Paolo Raiteri,[†] and Julian D. Gale[*,†]

[†]*Curtin Institute for Computation/The Institute for Geoscience Research (TIGeR), School of Molecular and Life Sciences, Curtin University, PO Box U1987, Perth, Western Australia 6845, Australia*

[‡]*Pawsey Supercomputing Centre, 1 Bryce Ave., Kensington, WA 6151, Australia*

E-mail: J.Gale@curtin.edu.au

Calcite surface structure

An alternative view of an island on the calcite $(1\,0\,\bar{1}\,4)$ surface is provided in Figure S1 in order to further illustrate the 16 distinct types of kink sites that can exist at the acute and obtuse steps. In this representation the atoms of the island are shown with a ball and stick representation, while those of the underlying terrace are omitted. The island is viewed from above the surface.

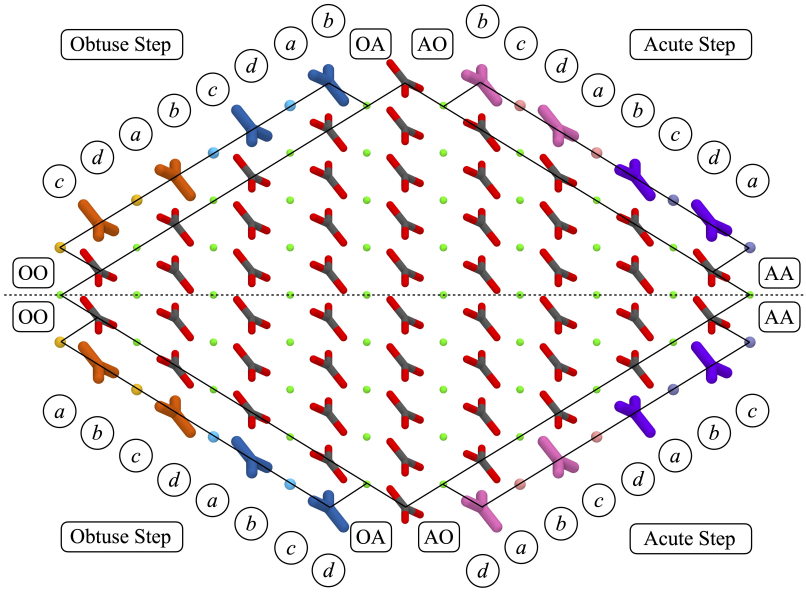

Figure S1: An island on the $(1\,0\,\bar{1}\,4)$ surface of calcite viewed at an angle to the surface showing the labels for each potential type of kink site where A and O indicate acute and obtuse, respectively. The labels a, b, c and d refer to the ion vertically above or below the label, as appropriate to the step edge. The glide plane parallel to $[\bar{4}\,\bar{2}\,1]$ is also indicated as this reduces the number of symmetry-unique kink sites. Atoms are colored green, gray and red for calcium, carbon and oxygen, respectively. Atoms at the step edge that form distinct types of kink site are highlighted in different colors.

Methods for LAMMPS simulations

To validate the molecular dynamics run with OpenMM, additional simulations were performed using LAMMPS[S1] with a time step of 1 fs, writing the atomic trajectories every

1 ps. The reciprocal space electrostatics were calculated using the PPPM algorithm[S2] with an accuracy of 10^{-5}. Bulk solids were first equilibrated at 1 bar and 300 K for 10 ns using the NPT ensemble and controlling the cell dimensions independently using their individual stress components. The temperature was controlled with a Langevin thermostat[S3] with a relaxation time of 0.1 ps and the pressure with a chain of 5 Hoover barostats with a relaxation time of 1 ps, using the correction of Martyna *et al.*[S4] The calcite–water interface was modelled by exposing the $(1\,0\,\overline{1}\,4)$ surface of calcite to a water layer containing 5,000 molecules, all contained within 3-D periodic boundary conditions. The calcite slab was 10 layers thick, measuring approximately 29 Å along z, the interface-normal direction, and having dimensions of 63 Å x 78 Å along x and y, respectively. Half of the top calcite layer was removed to produce two monomolecular steps parallel to the $\langle\overline{4}\,4\,1\rangle$ direction. The resulting acute and obtuse steps were approximately 28 Å apart. The slab in contact with the water layer was then equilibrated in the NPzT ensemble for 5 ns and the average cell calculated from the trajectory of this run measured about 59 Å along the z direction. Finally, half of the step was removed on both side of the upper terrace leading to a spacing of about 35 Å between opposite kinks (6 ion pairs along the step edge). Hence, four separate simulation cells were constructed with four different kink sites displayed (2 on the acute and 2 on the obtuse step) to generate the 16 unique types of kink on the $(1\,0\,\overline{1}\,4)$ surface. The kink cells had a total of 2,268 $CaCO_3$ formula units and were all equilibrated in the NVT ensemble for 5 ns before performing free energy calculations. The trajectories from these runs were used to calculate the average atomic positions for the atoms of the solid, which were employed for tethering specific atoms with harmonic oscillators, where required.

To determine the free energy of a specific ion or ion pair at a kink site interacting with the rest of the system, we used multistage free energy perturbation (FEP)[S5,S6] calculations, as implemented in LAMMPS, via the Bennett acceptance ratio (BAR) method[S7] using the pyMBAR code[S8] to determine the associated statistical uncertainties. The interactions of the perturbed ion with all other atoms were switched off in 96 stages of 5 ns each; 48

stages for the electrostatic interactions, followed by further 48 stages for the van der Waals interactions. For the calculation of the van der Waals term, we used a soft core repulsion to avoid singularities in the potential and forces when creating or annihilating particles.[S9] For the electrostatic part of the perturbation, the coupling parameter λ was varied between 0 and 1 using a constant increment. As observed in our previous study,[S10] halfway through the perturbation of the van der Waals parameters, water can often become trapped below the perturbed anion at kink sites, leading to a deterioration in the sampling of configurations. We therefore used a transformation according to a hyperbolic sine function to generate a non-uniform distribution for the van der Waals part of the perturbation, with more points concentrated around the value $\lambda = 0.5$. For kink site ions and ion pairs, 3-dimensional harmonic springs with a force constant of 1.5 eVÅ^{-2} were used to tether the perturbed ions to their initial positions to prevent diffusion away from the region of interest as the interactions are reduced. The same spring constant is also applied to the ion adjacent to the perturbed ion or ion pair and to the ion at the opposite kink further along the step edge. These additional restraints are necessary to prevent any ion from leaving the lower step edge (full dissolution is never observed but ions can move to the upper step edge) which can have a non-negligible influence on the computed free energy. All the atoms of carbonate ions were restrained rather than just the center of mass.

Non-equilibrium thermodynamic integration (TI) calculations were used to compute the free energies of adding or removing 3-dimensional harmonic springs to tether atoms to their initial positions, as described above. To achieve this, we used a modified version of the LAMMPS implementation of Freitas *et al.*[S11] as described in our previous work.[S10] Because carbonate is a molecular anion, an additional correction is required to go from the Einstein model to the species in the gas phase relative to our work on NaCl where only point ions were considered, which is to add the rotational free energy, in addition to the translational free energy, after removing the harmonic oscillator free energy for all atoms, as previously described above. To simplify this, the relative positions of the springs used to restrain the carbonate ion were

kept the same for all cases, such that the rotational free energy was a constant for all sites. For every case where TI was applied, 5 replica simulations were performed starting from different initial configurations in order to determine the statistical convergence of the free energy to introduce the restraints.

Free energy surfaces for restrained ion removal from kink sites at the calcite $(1\,0\,\overline{1}\,4)$-water interface

The free energy surface for ion removal from all kink sites with metadynamics using OpenMM was computed as a function of two collective variables, which were the surface normal distance from the ion's original position and the water coordination number of a calcium that is either the departing ion or the ion below a carbonate that is leaving the kink site, as described previously. All free energy curves were computed in the presence of a harmonic cylindrical restraint that limits the space explored in the plane of the surface such that the volume can be corrected to standard conditions. As a result, the free energy surfaces do not represent the actual pathway for ion removal, but instead provide an upper bound to any barriers on the unrestrained landscape. Here what is important is that the relative thermodynamics of the initial and final states are correctly determined (*i.e.* at the kink and in solution), which is independent of the pathway chosen. To compute this, the two-dimensional free energy landscapes (Figures S2 and S3) are post-processed to integrate out the water coordination collective variable to create the set of one-dimensional free energy curves (Figure S4). These are then analyzed according to the method of Doudou *et al.*[S12] to obtain the standard free energy difference.

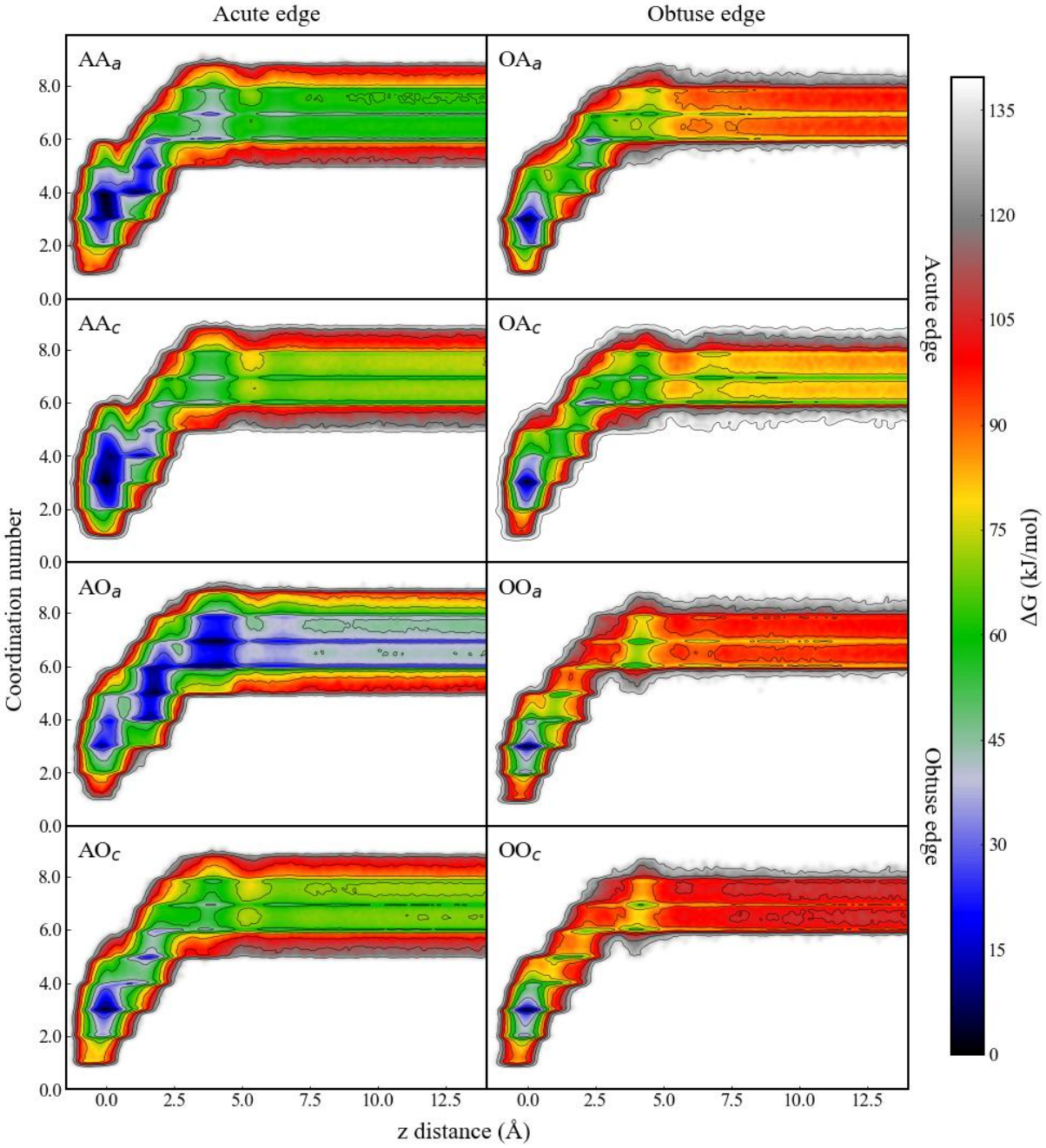

Figure S2: 2-Dimensional free energy profiles for each calcium kink ion as a function of the z distance (Å) normal to the surface of the slab and the water coordination number of the calcium ion as obtained from metadynamics. Each kink ion was restrained by a cylindrical harmonic potential with a radius of 0 Å.

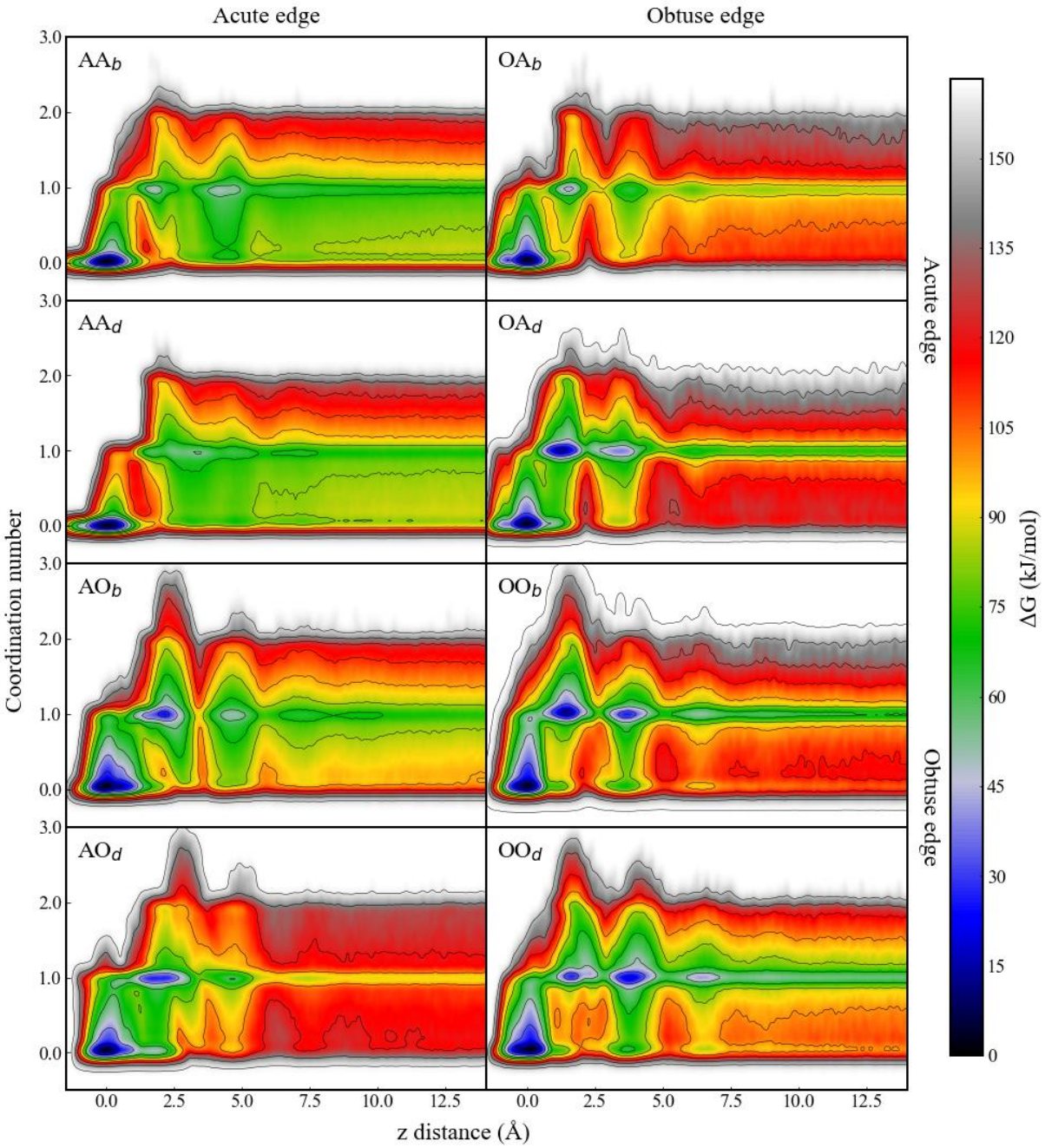

Figure S3: 2-Dimensional free energy profiles for each carbonate kink ion as a function of the z distance (Å) normal to the surface of the slab and the water coordination number of the calcium ion underneath the carbonate ion as obtained from metadynamics. Each kink ion was restrained by a cylindrical harmonic potential with a radius of 0 Å acting on the carbon of carbonate.

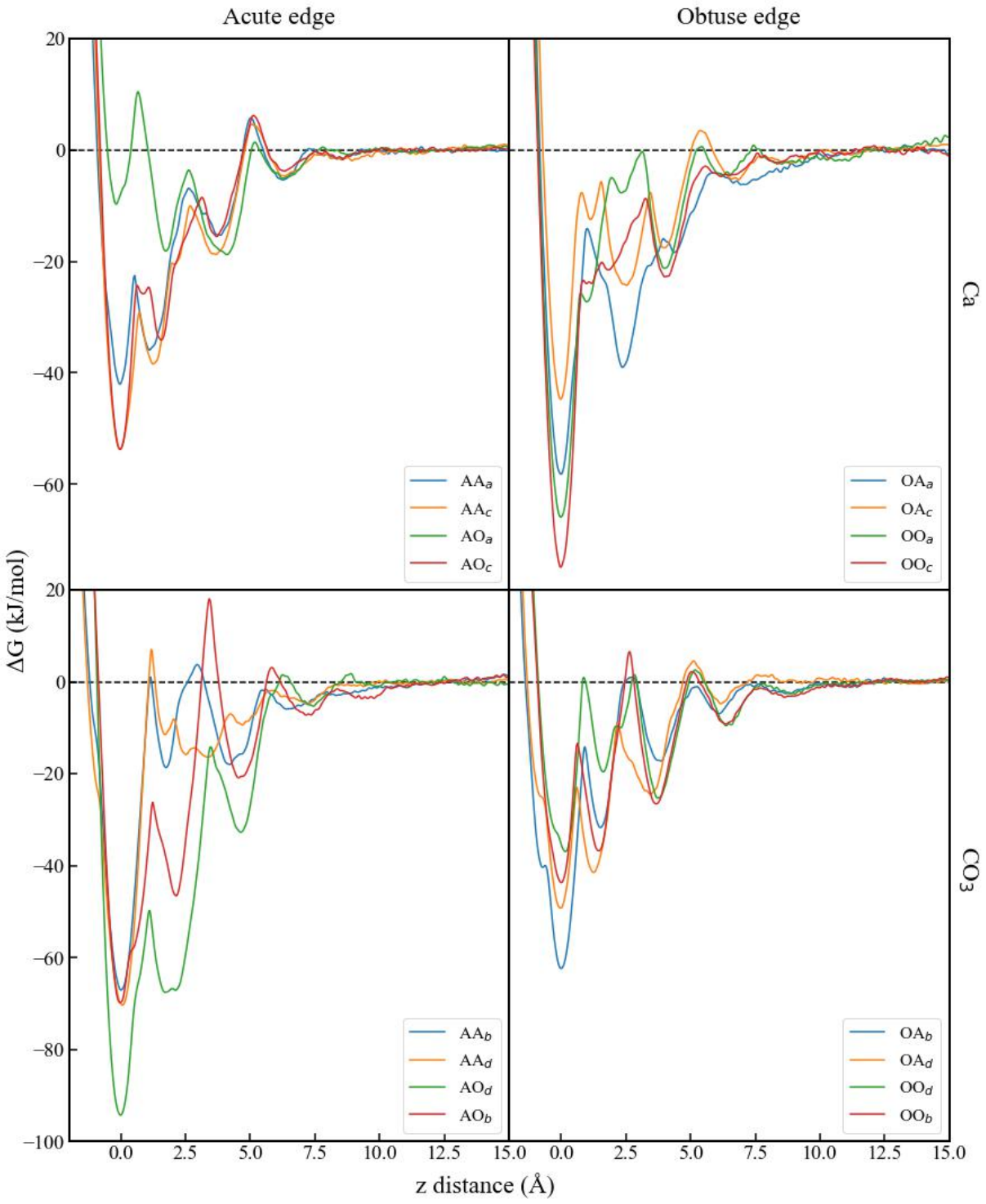

Figure S4: Free energy profiles for each kink ion as a function of the z distance (Å) normal to the surface of the slab (after integration out of the water coordination number) as obtained from metadynamics. Each kink ion was restrained by a cylindrical harmonic potential with a radius of 0 Å.

Components of the standard free energies for the alchemical cycle computed with OpenMM

The overall standard thermodynamics for kink sites as determined by alchemical removal of an ion to a 1 M solution using OpenMM is given in the main text as Table 1. Here we provide a breakdown of the components of the free energy in Table S1, both by contribution type and for the two different overall charge states of the slab used in the calculations that are averaged to reduce system size effects due to charge-charge interactions within periodic boundary conditions (see Silvestri *et al.*[S10] for details of this method).

Ideal kink site stabilities computed using LAMMPS

Table S2 shows the ideal ion dissolution standard free energy, ΔG_{diss}, as calculated using LAMMPS and the procedure highlighted in the earlier methods section. The free energy of dissolution is obtained by summing 1) the free energy, ΔG_{-Ion}, for transferring the ion from the kink site in contact with solution to vacuum as calculated by FEP; 2) the free energy, $\Delta G_{+springs}$, for adding springs on all atoms of the perturbed ion, plus the ion adjacent to the perturbed ion and the one at the opposite kink, as calculated by TI; 3) the free energy, $\Delta G_{-springs}$, for removing springs from all atoms of the ion adjacent to the perturbed ion pair and the one at the opposite kink as calculated by TI; 4) the corrections to the free energy accounting for the ion hydration (-1498.6±0.4 kJ/mol for Ca^{2+} and -1251.0±0.8 kJ/mol for CO_3^{2-}), the change of standard state from 1 atm to 1 M (7.95 kJ/mol), translation (-40.27 kJ/mol for Ca^{2+} and -41.78 kJ/mol for CO_3^{2-}) and, in the case of the carbonate ion, rotation (-25.6 kJ/mol). The ΔG_{diss} reported in the table are finally obtained by averaging the results from neutral and charged slab configurations. In comparing the results obtained from the thermodynamic cycle with LAMMPS with those obtained from OpenMM there is good agreement between the two sets of results (see Figure S5 for a graphical comparison): The

Table S1: Ideal kink site standard dissolution free energies (kJ/mol) calculated with OpenMM using free energy perturbation (FEP) at 300 K. This table provides the breakdown of the values given in the main text into the component terms to add and remove restraints by FEP ($\Delta G_{+spring}$ and $\Delta G_{-spring}$, respectively), to remove the restrained ion by FEP (ΔG_{-Ion}), and the sum of the remaining correction terms to complete the thermodynamic cycle (ΔG_{corr}).

Kink	System charge	ΔG_{-Ion}	$\Delta G_{+spring}$	$\Delta G_{-spring}$	ΔG_{corr}	ΔG_{diss}	$\langle \Delta G_{diss} \rangle$
AA_a	0	+1631.6	+5.2		−1525.5	+111.4	**+110.6**
	+2	+1630.9	+4.4			+109.9	
AA_b	0	+1233.9	+15.3	−5.4	−1306.8	−63.0	**−63.1**
	−2	+1233.7	+15.6	−5.8	−1306.8	−63.3	
AA_c	0	+1634.6	+4.3		−1525.5	+113.4	**+113.8**
	+2	+1635.7	+4.0			+114.2	
AA_d	0	+1231.0	+15.5	−4.3	−1306.7	−64.7	**−62.6**
	−2	+1236.2	+15.0	−4.8	−1306.6	−60.5	
AO_a	0	+1593.2	+8.7		−1525.5	+76.4	**+76.5**
	+2	+1596.0	+6.1			+76.6	
AO_b	0	+1230.6	+22.7	−5.4	−1306.7	−58.6	**−61.8**
	−2	+1230.0	+15.4	−3.8	−1306.6	−65.0	
AO_c	0	+1645.0	+3.9		−1525.5	+123.4	**+124.5**
	+2	+1646.6	+4.5			+125.7	
AO_d	0	+1259.2	+13.9	−7.9	−1306.8	−41.7	**−42.9**
	−2	+1257.2	+13.2	−7.9	−1306.7	−44.2	
OA_a	0	+1650.1	+3.7		−1525.5	+128.3	**+127.6**
	+2	+1648.7	+3.6			+126.8	
OA_b	0	+1233.3	+15.1	−6.1	−1306.8	−64.5	**−65.4**
	−2	+1231.5	+15.6	−6.3	−1307.1	−66.3	
OA_c	0	+1633.6	+3.8		−1525.5	+111.9	**+111.3**
	+2	+1632.3	+4.0			+110.7	
OA_d	0	+1220.6	+15.3	−4.6	−1306.7	−75.7	**−76.1**
	−2	+1219.6	+15.5	−4.8	−1306.9	−76.6	
OO_a	0	+1659.2	+4.0		−1525.5	+137.7	**+137.0**
	+2	+1657.5	+4.3			+136.4	
OO_b	0	+1210.8	+16.3	−4.1	−1306.9	−83.9	**−87.2**
	−2	+1204.9	+16.1	−4.5	−1306.8	−90.4	
OO_c	0	+1664.6	+3.4		−1525.5	+142.5	**+142.5**
	+2	+1663.9	+4.2			+142.5	
OO_d	0	+1205.2	+23.9	−4.4	−1312.5	−87.8	**−89.4**
	−2	+1198.8	+21.2	−5.1	−1307.5	−92.6	
$2 \times \langle \langle \Delta G_{diss} \rangle \rangle$							**+48.9**

mean absolute deviations for the calcium and carbonate kink sites are 3.6 and 4.0 kJ/mol, with the largest discrepancy for any single site being 5.9 kJ/mol. However, the difference in the values when averaged over kink site types is far smaller and within the statistical uncertainties of the method, indicating that there is no systematic offset in the values.

Ion pair stabilities at kink sites

As a further check on the correctness of the free energies, the thermodynamics of removing all possible ion pairs from the kink sites at standard conditions were also computed using FEP with LAMMPS. The procedure follows that above for the individual ions except that 2 ions are removed simultaneously. The results for the ion pair stabilities are given in Table S3. Here it is important to note that there is no difference between the real and ideal values since there is no contribution from the interfacial potential when removing the charge-neutral ion pairs. As found for the individual ion removals, the average dissolution free energy over all ion pairs ($+49.0 \pm 0.8$ kJ/mol) is in excellent agreement with the bulk dissolution free energy for the force field ($+48.4$ kJ/mol). Similarly, ion pairs at kinks on the obtuse step have a slightly higher degree of stability on average by 1.25 kJ/mol, though the variation between ion pair types is greater than this with ion pairs at the AA and OO kink types being more stable than the mixed combinations of A and O.

Interfacial potential at the halite (001)-water interface

For comparison with the calcite results, the interfacial potential at the interface between NaCl (halite) and water was computed for the dominant (001) surface. This was to allow the comparison of the interfacial potential contribution to the kink site energies, as previously determined by Silvestri *et al.*,[S10] with the full potential across the flat interface. The same approach was used as described for the calcite-water interface in the main text. Here the aqueous sodium chloride system was modelled using the same force field as per Silvestri

Table S2: Ideal kink site standard dissolution free energies (kJ/mol) calculated with LAMMPS using the combination of free energy perturbation to remove an ion (ΔG_{-Ion}) and thermodynamic integration to add or remove restraints ($\Delta G_{+springs}$ and $\Delta G_{-springs}$, respectively) at 300 K.

Kink	System charge	ΔG_{-Ion}	$\Delta G_{+spring}$	$\Delta G_{-spring}$	ΔG_{corr}	ΔG_{diss}	$\langle \Delta G_{diss} \rangle$
AA_a	0	+1640.9±0.1	+27.8±1.7	−36.1±2.1	−1525.5	+107.1±2.7	**+108.0±1.5**
	+2	+1643.6±0.1	+20.7±0.3	−29.8±0.8		+109.0±1.0	
AA_b	0	+1238.4±1.4	+21.0±2.0	−14.3±2.0	−1307.0	−61.8±3.2	**−65.4±2.2**
	−2	+1233.3±1.7	+47.6±1.5	−42.8±1.7		−68.9±3.0	
AA_c	0	+1648.4±0.1	+22.1±0.2	−41.0±0.9	−1525.5	+104.0±2.0	**+108.1±1.4**
	+2	+1650.8±0.1	+20.0±0.6	−33.1±1.9		+112.2±2.0	
AA_d	0	+1241.1±0.9	+17.7±0.4	−7.8±0.4	−1307.0	−56.0±1.3	**−56.7±1.5**
	−2	+1235.7±1.1	+33.9±1.2	−19.8±1.8		−57.3±2.6	
AO_a	0	+1608.5±0.1	+25.2±0.3	−29.9±1.7	−1525.5	+78.3±1.8	**+75.7±1.2**
	+2	+1609.5±0.1	+17.9±0.4	−28.9±1.3		+73.1±1.5	
AO_b	0	+1233.7±0.9	+25.5±1.8	−11.0±0.6	−1307.0	−58.7±2.3	**−56.0±1.6**
	−2	+1240.3±0.5	+44.8±0.5	−31.5±1.6		−53.3±1.9	
AO_c	0	+1648.7±0.1	+31.5±1.7	−44.4±1.9	−1525.5	+110.2±2.6	**+119.1±2.0**
	+2	+1653.0±0.1	+40.0±2.1	−40.6±2.0		+127.8±2.9	
AO_d	0	+1260.2±1.5	+14.8±0.4	−10.1±0.5	−1307.0	−42.1±1.8	**−40.6±1.7**
	−2	+1262.1±2.1	+38.6±1.1	−32.9±0.9		−39.2±2.7	
OA_a	0	+1662.1±0.1	+25.1±0.2	−37.1±0.6	−1525.5	+124.6±0.8	**+125.4±0.6**
	+2	+1664.0±0.1	+14.9±0.2	−27.2±0.7		+126.2±0.8	
OA_b	0	+1236.5±2.4	+17.4±0.3	−7.7±0.1	−1307.0	−60.7±2.6	**−62.3±1.8**
	−2	+1233.8±2.0	+33.8±0.3	−24.5±1.0		−63.8±2.3	
OA_c	0	+1645.5±0.1	+26.5±0.4	−42.1±0.9	−1525.5	+104.4±1.0	**+106.8±0.7**
	+2	+1645.7±0.1	+17.5±0.2	−28.5±0.3		+109.2±0.6	
OA_d	0	+1216.3±1.9	+16.5±0.6	−6.9±0.1	−1307.0	−81.1±2.2	**−79.9±0.9**
	−2	+1219.3±1.9	+32.7±0.2	−23.8±0.5		−78.7±2.1	
OO_a	0	+1664.7±0.1	+24.1±0.3	−30.8±0.5	−1525.5	+132.5±0.7	**+133.5±0.5**
	+2	+1667.0±0.1	+16.5±0.2	−23.6±0.3		+134.4±0.6	
OO_b	0	+1210.2±1.9	+12.2±0.3	−5.8±0.1	−1307.0	−84.4±2.1	**−81.8±1.6**
	−2	+1215.8±1.7	+38.9±0.6	−27.0±0.7		−79.3±2.1	
OO_c	0	+1668.4±0.1	+25.7±0.4	−31.0±0.3	−1525.5	+137.6±0.6	**+137.9±0.5**
	+2	+1669.8±0.1	+8.3±0.1	−24.4±0.5		+138.2±0.6	
OO_d	0	+1206.5±1.3	+18.2±0.9	−6.6±0.1	−1307.0	−88.9±1.7	**−85.9±1.5**
	−2	+1213.8±1.7	+38.9±1.2	−28.5±0.5		−82.8±2.2	
$2 \times \langle \Delta G_{diss} \rangle$	AA						**+47.1±2.4**
	AO						**+49.1±2.3**
	OA						**+45.0±1.6**
	OO						**+51.8±1.6**
$2 \times \langle \langle \Delta G_{diss} \rangle \rangle$							**+48.3±1.0**

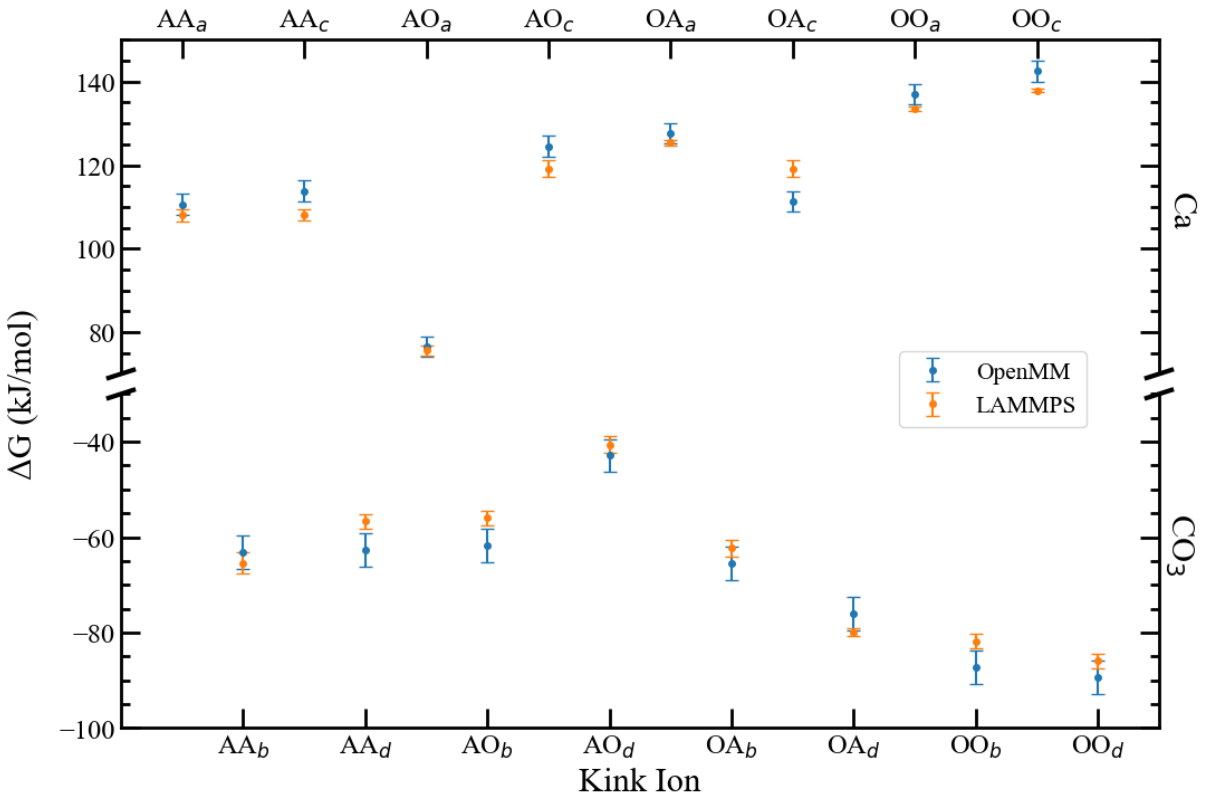

Figure S5: Graphical comparison between the ideal standard kink ion dissolution free energies as computed from OpenMM and LAMMPS. The error bars represent the 95% confidence intervals presented in the manuscript and Table S2.

Table S3: Ion pair standard dissolution free energies (kJ/mol) calculated with LAMMPS using the combination of free energy perturbation to remove ions (ΔG_{-IP}) and thermodynamic integration to add or remove restraints ($\Delta G_{+springs}$ and $\Delta G_{-springs}$, respectively) at 300 K. The notation for ion pairs at kinks follows that given in the main text for ions except that there are 2 letters from a, b, c and d, to denote the combination of ions.

	Kink	ΔG_{-IP}	$\Delta G_{+springs}$	$\Delta G_{-springs}$	ΔG_{diss}
	AA_{ad}	+2873.3±0.7	+32.5±1.1	-21.4±1.0	**+52.0±1.9**
	AA_{bc}	+2871.0±3.2	+37.9±0.7	-27.5±1.3	**+48.9±3.6**
	AO_{ab}	+2847.4±2.1	+37.7±1.4	-18.2±1.3	**+34.5±3.0**
	AO_{cd}	+2872.2±0.5	+51.2±1.9	-32.7±0.6	**+58.2±2.2**
	OA_{ab}	+2867.1±1.4	+26.1±0.7	-24.9±0.2	**+35.9±1.0**
	OA_{cd}	+2880.9±0.6	+39.0±0.5	-27.2±0.5	**+60.2±1.3**
	OO_{ab}	+2871.1±2.0	+26.0±0.2	-15.2±0.3	**+49.5±2.2**
	OO_{cd}	+2871.1±0.3	+40.8±0.5	-26.4±0.3	**+53.1±1.1**
$\langle \Delta G_{diss} \rangle$	AA				**+50.4±2.0**
	AO				**+46.4±1.9**
	OA				**+48.0±1.1**
	OO				**+51.3±1.3**
$\langle\langle \Delta G_{diss} \rangle\rangle$					**+49.0±0.8**

et al., namely the Joung-Cheatham model[S13] for NaCl combined with SPC/E water. The electric potential as a function of the surface normal z distance was averaged over the course of 10 ns for a ∼66 Å thick slab of halite equilibrated in contact with a layer containing 2,399 water molecules. All ensemble, thermostat and barostat settings used during the construction of the NaCl-water slab were as per the case of calcite-water. Three replica simulations were performed from different initial starting positions and velocities in order to estimate the statistical uncertainty in the final result. The computed potential versus position is illustrated in Figure S6, resulting in a calculated interfacial potential of -0.088 ± 0.008 V (presented as a 95% confidence interval).

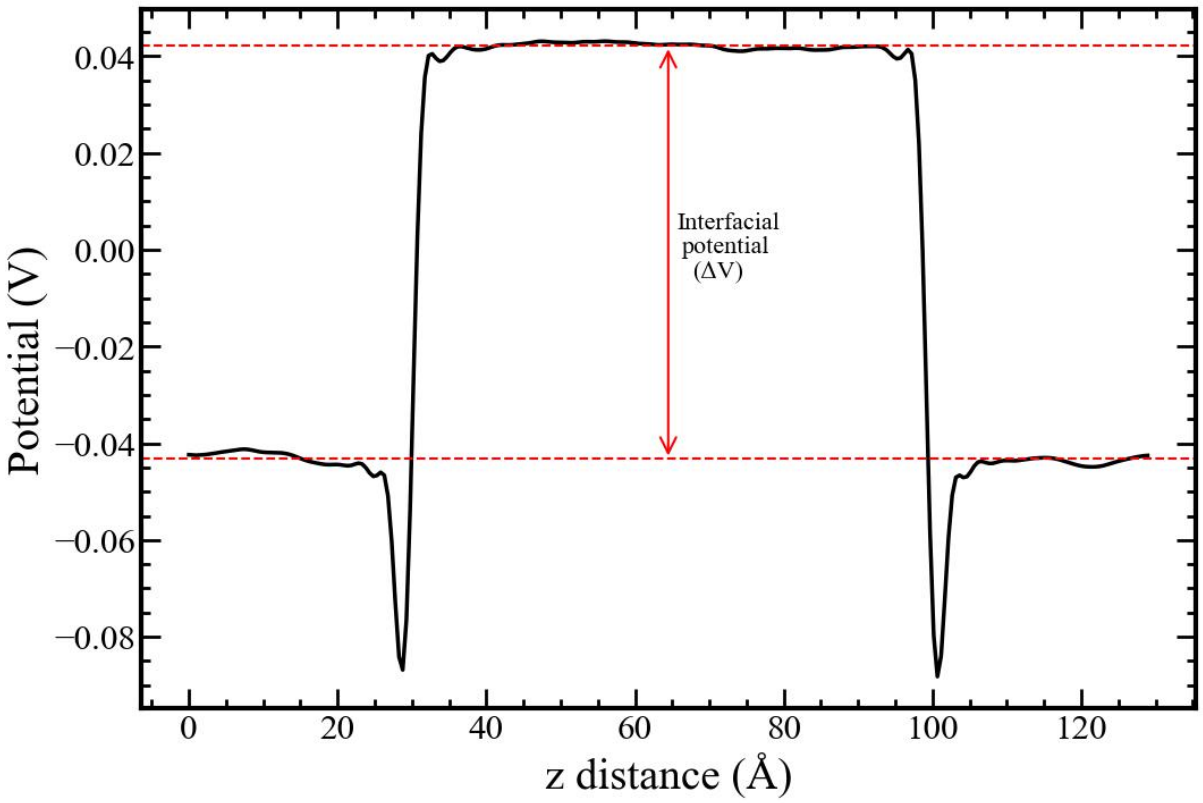

Figure S6: Electric potential as a function of the surface normal z distance for the halite (001)-water interface.

References

(S1) Plimpton, S. Fast Parallel Algorithms for Short-Range Molecular Dynamics. *Journal of Computational Physics* **1995**, *117*, 1–19.

(S2) Hockney, R. W.; Eastwood, J. W. *Computer Simulation Using Particles*; Adam Hilger, NY, 19889.

(S3) Schneider, T.; Stoll, E. Molecular-dynamics study of a three-dimensional one-component model for distortive phase transitions. *Phys. Rev. B* **1978**, *17*, 1302–1322.

(S4) Martyna, G. J.; Tobias, D. J.; Klein, M. L. Constant Pressure Molecular Dynamics Algorithms. *The Journal of Chemical Physics* **1994**, *101*, 4177–4189.

(S5) Kirkwood, J. G. Statistical mechanics of fluid mixtures. *The Journal of Chemical Physics* **1935**, *3*.

(S6) Zwanzig, R. W. High-Temperature Equation of State by a Perturbation Method. I. Nonpolar Gases. *Journal of Chemical Physics* **1954**, *22*.

(S7) Bennett, C. H. Efficient estimation of free energy differences from Monte Carlo data. *Journal of Computational Physics* **1976**, *22*.

(S8) Shirts, M. R.; Chodera, J. D. Statistically optimal analysis of samples from multiple equilibrium states. *Journal of Chemical Physics* **2008**, *129*.

(S9) Beutler, T. C.; Mark, A. E.; van Schaik, R. C.; Gerber, P. R.; van Gunsteren, W. F. Avoiding Singularities and Numerical Instabilities in Free Energy Calculations Based on Molecular Simulations. *Chemical Physics Letters* **1994**, *222*, 529–539.

(S10) Silvestri, A.; Raiteri, P.; Gale, J. D. Obtaining Consistent Free Energies for Ion Binding at Surfaces from Solution: Pathways versus Alchemy for Determining Kink Site Stability. *Journal of Chemical Theory and Computation* **2022**, *18*, 5901–5919.

(S11) Freitas, R.; Asta, M.; de Koning, M. Nonequilibrium Free-Energy Calculation of Solids Using LAMMPS. *Computational Materials Science* **2016**, *112*, 333–341.

(S12) Doudou, S.; Burton, N. A.; Henchman, R. H. Standard Free Energy of Binding from a One-Dimensional Potential of Mean Force. *Journal of Chemical Theory and Computation* **2009**, *5*, 909–918.

(S13) Joung, I. S.; Cheatham, T. E. Determination of Alkali and Halide Monovalent Ion Parameters for Use in Explicitly Solvated Biomolecular Simulations. *The Journal of Physical Chemistry B* **2008**, *112*, 9020–9041.